Dear Dr. Zellweger,
On behalf of all co-authors, I hereby submit a revised version of our manuscript "Accurate measurements of atmospheric carbon dioxide and methane mole fractions at the Siberian coastal site Ambarchik". We addressed all comments made in both reviews that the manuscript received in replies to the individual reviews. We would like to thank both referees for their constructive criticism and are confident that we addressed all comments satisfactorily. In addition, we made a few minor changes to improve the flow of the manuscript, remove some typos and highlight ongoing efforts to ensure the accuracy of the data obtained at Ambarchik. Below we include both previously published responses to the reviews and the revised manuscript with changes to the initially submitted version highlighted.
With best regards on behalf of all co-authors,
Friedemann Reum

Author's response to review 1

This paper by Reum et al., presents a new atmospheric observatory for CO2 and CH4 in the Siberian coastline. The presence of this new research infrastructure is a very valuable opportunity for the atmospheric science community, especially taking into account the possible role that carbon stocks in the artic region (i.e. permafrost melting) can play in the next decades under the current climate change.

Performing such high level quality measurements in remote regions is not an easy task and strong scientific and technical skills are necessary to obtain reliable data with dense time coverage (as needed to perform inversion for GHG emission studies)

The authors describe with good details the experimental set-up adopted for CO2 and CH4 measurements as well as methods for data correction and data screening. Very basic analysis of the first months of data are provided.

Even if the methods adopted in this paper are not innovative, I think that the availability of this new station (and related data-sets) is a matter of interest for the atmospheric community.

Personally, I have some concerns about the design of the gas handling system and the data screening. For these reasons, I ask the authors for providing more explanation or details for some specific points (listed in the following) before publication.

SPECIFIC COMMENTS

"2.3 Gas Handling"Any kind of rain guard was mounted on the air inlet?

Yes, the air inlets used for our station come with a rain guard. They are shown pictographically in Fig. 3, and we add "Air inlets *with rain guards*" to the text.

The air flow diagram presents a very complicate system, with a number of connections and valves which increase the possibility of leaks and dead volumes. Even if I do not see anything wrong in this set-up, nonetheless I'm wondering why a so-complex system was adopted.

The basic concept behind this arguably complicated setup was to be less dependent on the rotary valve. More details on this choice are given three comments below.

For this reason, I'm wondering if the authors performed specific leak test on the system. If yes, what kinds of test have been carried out? Are these tests repeated routinely?

Avoiding leakage was a top priority during assembly of the gas handling system. Leak tests have been carried out, but were omitted in the manuscript for the sake of brevity. In the revised manuscript, we include them as part of Sect. 2.3 ("Gas handling"). In short, leak tests were performed by evacuating the gas handling system and observing the pressure increase over several hours. Leak rates determined this way were found to be negligible. During later maintenance visits, only simple breathing tests were performed to avoid opening tubing connections.

By using two flushing pump for each sampling lines you would avoid the complex switching

system downstream of the antiparticulate filters F4-F3.

We use only one flushing pump to minimize power consumption of the measurement system, which is an important consideration at this remote site.

I'm also wondering why you didn't use a rotary valve with more inputs to manage also the ambient air: this would have the advantage of simplifying the system (less possibility of leaks) and use a larger part of sampling circuit for both ambient air and calibration/target gas measurements with clear advantages and effectiveness for application of calibration and evaluation of target gas results.

This setup would in principle be possible and would indeed have the advantages that the reviewer pointed out. However, our setup minimizes the workload put on the Valco valve. This is an advantage because the rotor of the Valco valve is a consumable that, for top performance, has to be exchanged regularly, particularly if switched frequently. This is not a trivial task that only well-trained personnel can perform. One may alternatively exchange the Valco valve completely, but this would introduce additional risk of leaks, as all connections on the Valco would have to be opened. In our setup, the Valco valve switches position about twice per day. In the setup suggested by the reviewer, the Valco valve would, in addition, be used for switching between the two inlet lines from the tower, i.e. six times per hour. For the above reasons, we chose to avoid this workload.

Please provide the residence time of sampling within the system.

The full residence time is on the order of 12 sec. We add this information to the Sect. 2.3 ("Gas handling").

No water traps are used along the ambient inlet lines. In the paragraph 3.2 you mentioned that "longer probing time of the first tank serves to flush residual water out of the tubing". Do you mean that water are present in the tubing? Is this due to condensation or drizzle sampling? In both case this can represent a problem since the presence of liquid water can create artifact in the measurement. Please explain and comment.

This statement refers to residual water *vapor* due to washing out water molecules adhering to the tubing wall. We clarify the sentence to avoid misunderstandings.

"3.1 Water correction"

It is possible to add in the supplementary material more info about the water vapour test? E.g. plot of Concentration(wet)/Concentration(dry) ratios plotted as function of water vapour level for CO2 and CH4 or time series of CO2wet, CH4wet during the water correction experiment. I'm wondering which is the absolute difference (in ppm and ppb for CO2 and CH4) if the "classical" water droplet experiment is used instead the Reum et al. (20q8) procedure. I'm pretty sure that this difference is well lower than the WMO compatibility goals.

First a clarification: we originally cited the discussion paper Reum et al. (2018). In the meantime, the final revised paper was published, so we update the reference throughout this response and in the revised manuscript.

Differences between the water correction methods were documented in Reum et al. (2019), where they were up to 50 % of the WMO inter-laboratory compatibility goal for CO2 and up to 80 % that goal for CH4. Thus, the differences were smaller than the WMO goals, as suggested by the reviewer. However, the value of the new method is due to the fact that the WMO goals refer to overall compatibility, which suffers from other errors.

We think that the differences between the methods are documented in enough detail in Reum et al. (2019). However, perhaps we have not communicated clearly enough that data from Ambarchik were used therein: the gas washing bottle experiments in 2015 and 2017 were analyzed in Reum et al. (2019) to evaluate the new method, and the CRDS analyzer in Ambarchik is the one labeled "Picarro #5" in Reum et al. (2019). In the revised manuscript, we add a note to the main text and Appendix B about this correspondence, so that the interested reader can find additional details in Reum et al. (2019). As documented in the manuscript, a direct comparison of the two experimental methods (gas washing bottle vs droplet) with the Ambarchik system may be conflated with drift, because droplet measurements were only done in February and July 2014, whereas the gas washing bottle method was used in 2015. A more direct comparison of the methods based on data from a different Picarro analyzer can be found in Reum et al. (2019).

The requested plot of wet air- over dry air mole fractions is given below (Fig. 1). However, as the reviewer pointed out, the differences between the methods are small and hardly visible in this type of plot. Because of this, and since the gas washing bottle data were presented in more detail in Reum et al. (2019), we chose to present the differences between the experiments with the Ambarchik system as in Fig. 4 in our manuscript. The plot below is not suitable to present the differences between the methods. Therefore, we prefer not to include it in the manuscript.

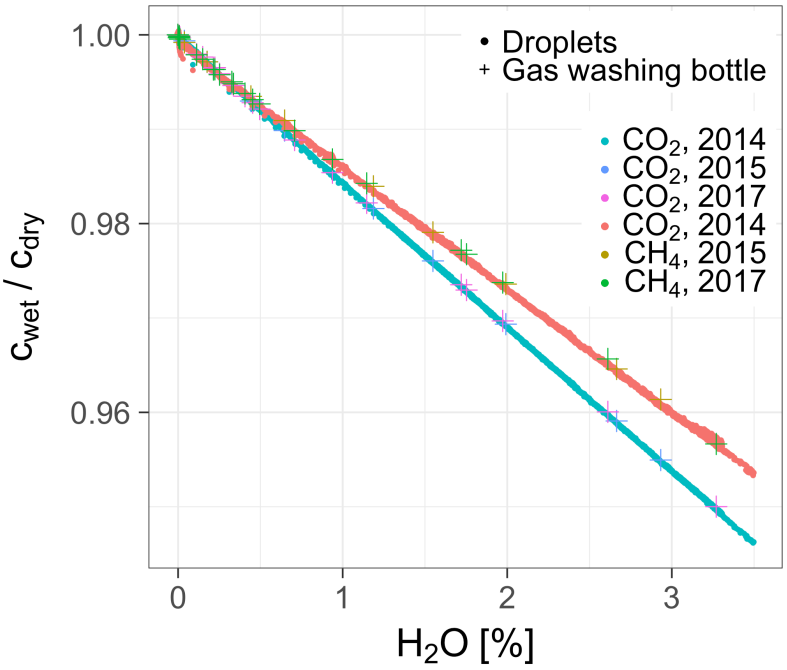

Fig. 1: Wet air mole fractions vs water vapor from the water correction experiments presented in the main text of the manuscript. The data from the three droplet experiments are shown with the same color.

The requested time series are plotted below (Fig. 2). As above, we think that this material is too much to be included in the manuscript.

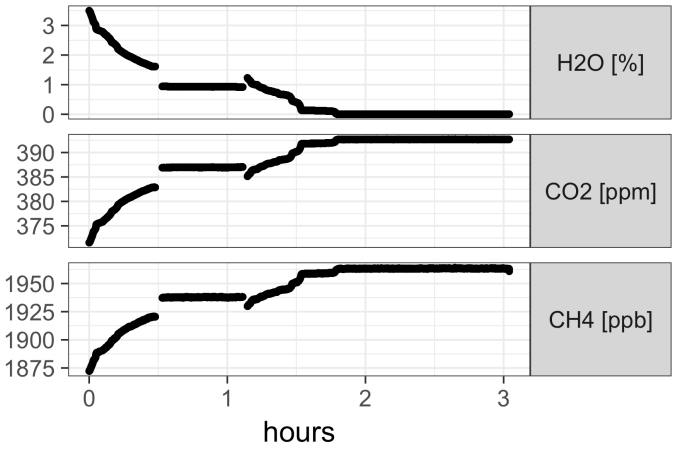

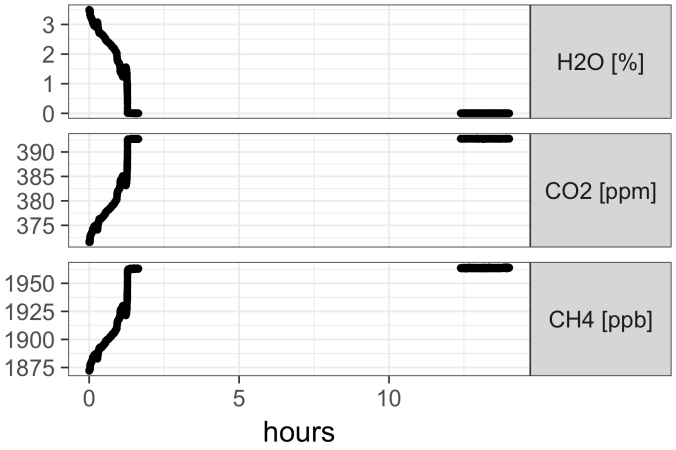

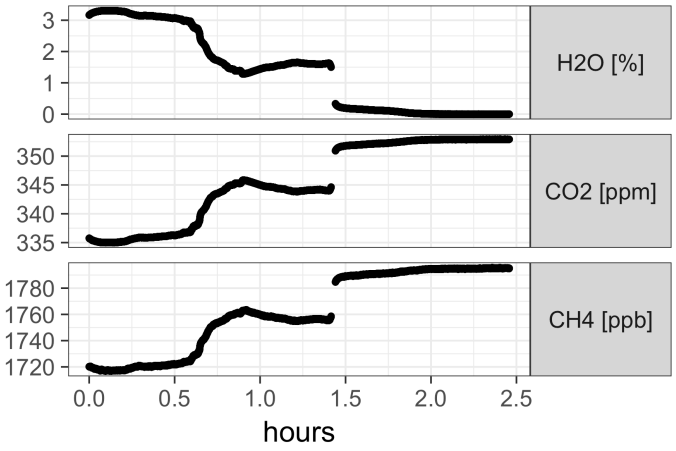

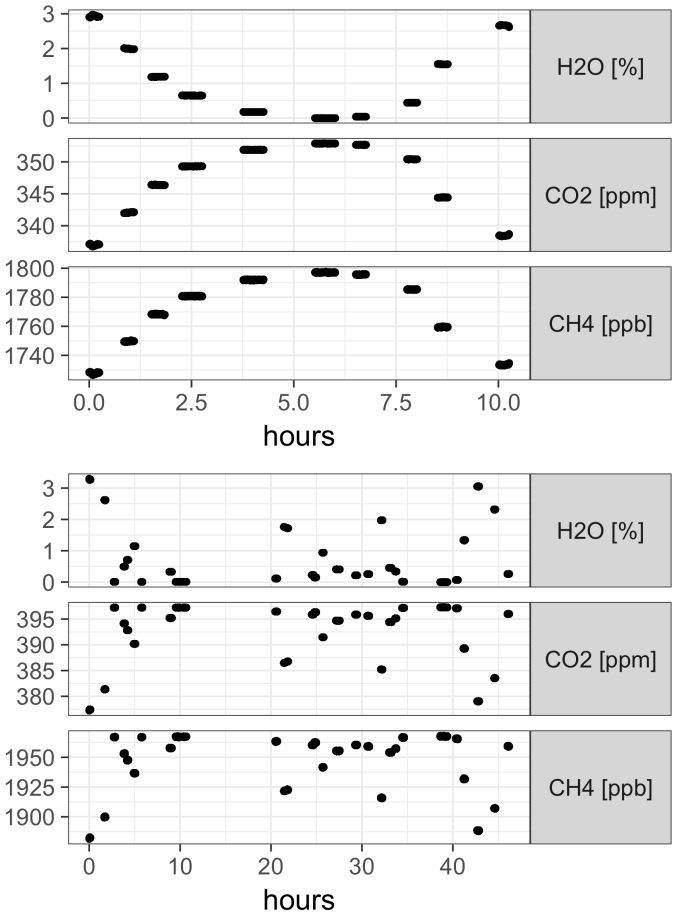

Fig. 2: Time series of water vapor, CO_2 and CH_4 mole fractions during all water correction experiments. Only data used for inferring water correction functions are shown. Panels 1-3: droplet experiments conducted in 2014. Panels 4-5: Gas washing bottle experiments conducted in 2015 and 2017, respectively.

Line 19: Did you apply the same correction for all the data series by considering an average value of the correction coefficients derived during each single experiment? This approach will become unfeasible when many years of measurements will be available, I suppose.

Yes, as documented in the manuscript, an average correction was applied because the data so far do not allow deriving trends in the water correction. For the future, we plan to include the influence of potential trends, but this can only be implemented when more experiments become available. As we see it, this strategy is the most practical solution at this point.

How much would change CO2 and CH4 correction if results from single experiments are used?

The variability in the output based on single experiments was shown in Fig. 4 in the manuscript. Differences were up to 0.14 ppm CO2 and 1.2 ppb CH4. These maximum differences occur at 3 % H2O and 2.3 % H2O for CO2 and CH4, respectively. Note that ambient H2O mole fractions in Ambarchik rarely exceed 1.5 % H2O. In this domain, the differences between the water correction experiments are smaller.

Figure 4 and Figure 5: the WMO goals are wrong in these figures. They are +/- 0.1 ppm for CO2

and +/- 2 ppb for CH4.

In the revised manuscript, we adopt the captions by Reum et al. (2019). In short, these should be thought of as the WMO internal reproducibility goals. The WMO inter-laboratory compatibility goals as cited by the reviewer refer to differences between data from different laboratories. However, keeping the accuracy with respect to a common calibration scale, which is what plots depict, within these thresholds does not ensure achieving this goal. Consider CO2 data from two stations. One has a positive bias of +0.1 ppm CO2, while the other has a negative bias of -0.1 ppm CO2 with respect to their common calibration scale. Thus, the bias between these two stations is 0.2 ppm CO2, exceeding the interlaboratory compatibility goal. However, keeping the accuracy with respect to the calibration scale within half of the WMO inter-laboratory compatibility goal ensures that biases between stations do not exceed them. Therefore, we chose these goals as context for the accuracy of our measurements with respect to the WMO calibration scales (i.e. water correction and calibration, Fig. 4 and 5, respectively). The WMO refers to these goals as the "internal reproducibility goals" (WMO, 2016).

We make this point clearer by adding a short version of this paragraph to the text where Fig. 4 is introduced, and by modifying the labels in the figures from "Range covering WMO goal" to "WMO internal reproducibility goal".

"3.2 Calibration"

How many measurement cycles are carried out during each calibration event?

One calibration event consists of one cycle of three tank measurements, in order High – Middle – Low. We clarify this in the revised manuscript. Note that data are calibrated based on a weighted average of about 25 such events. Note also that it's important to assess whether the order of gas tank measurements affects the results. We discussed tests with reversed order of the tanks in Appendix E.3 (E.4 in the revised manuscript). Based on these data, we could not rule out the presence of small biases, but determined that their impact on calibrated data would be small. Therefore, we consider our calibration strategy to be adequate. As stated in the Appendix, we nonetheless plan to rule out these small potential errors with additional experiments in the future.

Did you apply any metric to evaluate the success of the calibration (e.g. standard deviation of single injection or data coverage).

In our opinion, the scatter of raw CO2 and CH4 data observed during calibrations as well as of the derived fitted coefficients is the best indicator of the precision of the calibration procedure. These data are also manually checked for outliers.

Did you consider stabilization time after starting of the single cylinder injection?

Yes, we investigated whether the gas tank measurements are sufficiently stabilized based on two methods. One was to fit an exponential stabilization function to the average of all measurements of each tank doing this with individual measurements was not robust because the signal was. We then compared the fitted equilibrium mole fractions to the average mole fractions of the last two minutes per tank (i.e., the values that were used to calibrated data). As reported in Appendix E.3 (E.4 in the revised manuscript), the differences were negligible. The other method was to

measure the tanks on site for up to two hours. As reported in Appendix E.3 (E.4 in the revised manuscript), there were small variations of CO2 and CH4, but no consistent drifts over the full span of the experiments. Therefore, we think that the worst-case numbers given in the manuscript, which are well below 0.1 ppm CO2 and 2 ppb CH4, do not indicate insufficient stabilization. As stated in the Appendix, we nonetheless plan to rule these small potential errors out with additional experiments in the future.

How do you handle the fitting of calibration parameters when discontinuity of data appear (e.g. instrument switch off/on).

The regular operation period of the instrument without switching it on/off is usually very long (several months) since both on-site maintenance and power supply are very reliable under normal conditions. However, particularly during the start-up period of the site, when minor flaws in the setup still needed to be straightened out, the system sometimes needed to be restarted more than once a week. Even then, discontinuities in instrument drift (Fig. 5) were not observed, so we are confident that the record is not affected by discontinuities. Thus, discontinuities like analyzer restarts are not explicitly accounted for.

Can you provide the time series of standard deviation (based on 1-minute averages) of single target measurements (a measure for the CMR) and the time series of the standard deviation over 72 hours of the target gas injection means (LTR)?

We provide the requested quantities and plots here. However, in our opinion, they express similar uncertainties as already accounted for and quantified in our uncertainty estimates. In addition, they reflect neither our calibration strategy nor the averaging strategy (i.e. hourly averages). Therefore, we prefer not to include them in the revised manuscript.

In Yver Kwok et al. (2015), CMR and LTR were defined as average values, not as timeseries. Here, we first provide values according to those definitions, and then time series as requested by the reviewer. We did not perform measurements that follow precisely the protocol in Yver Kwok et al. (2015). However, a similar value as LTR is already incorporated in our uncertainty estimates: as stated in Appendix E, analyzer drift and precision ($\sqrt{{u_p}^2 + {u_b}^2}$) were jointly estimated from a dry air measurement in the lab prior to field deployment that lasted 12 days. More precisely, analyzer drift and precision of hourly values were calculated as the standard deviation of hourly averages over this 12-day measurement and was reported in the manuscript (0.013 ppm CO2, 0.25 ppb CH4). This is somewhat similar to the LTR by Yver Kwok et al. (2015), which was defined as the standard deviation of 10-min averages over a period of 3 days. Alternatively, one may use the regular target gas injections for computing a measure for LTR. To obtain a meaningful standard deviation, more than 72h have to be considered, since measurements take place only every 29h. Therefore, we show the timeseries of the standard deviation over 13 days, which corresponds to 11 regular Target tank measurements. We use the averages of the final 2 min of each target tank measurement that were used to calibrate data (Fig. 3). The average LTR estimated this way is 0.018 ppm CO2 and 0.25 ppb CH4.

From the same 12-day measurement used to estimate analyzer drift and precision, CMR may be calculated as standard deviation of raw data within 1-minute intervals. In 30-h intervals, they were on average 0.015 ppm CO2 and 0.17 ppb CH4. This is shown in Fig. 4 for one 30-h interval.

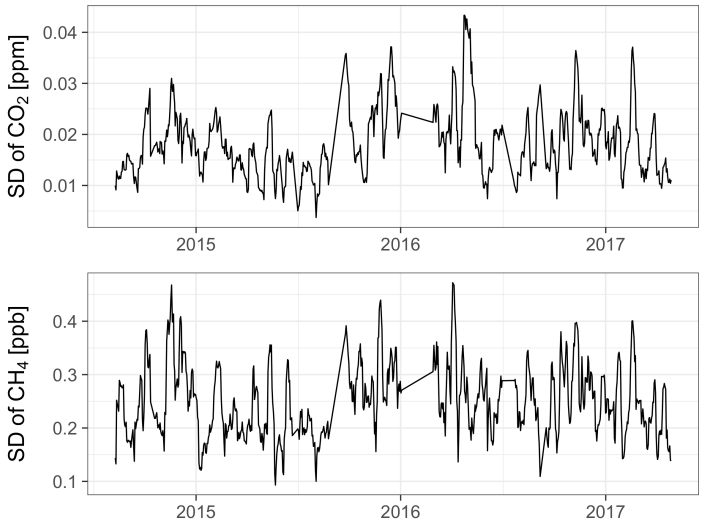

Fig. 3: Running standard deviations of Target tank data averaged over 13 days (used for estimating LTR).

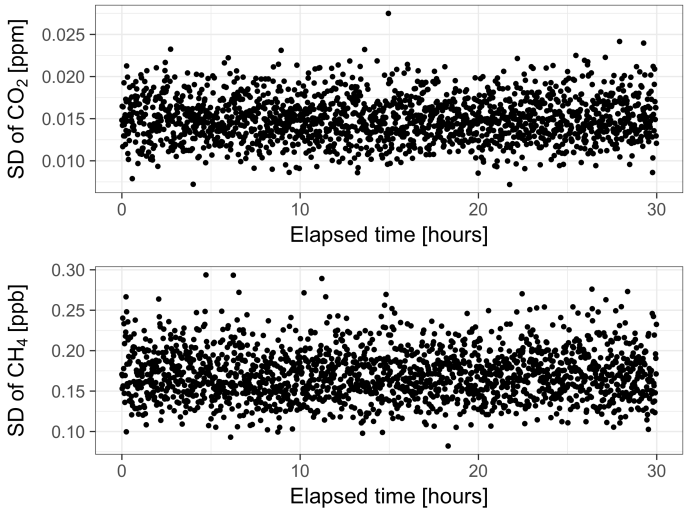

Fig. 4: Timeseries of standard deviation of 1-min averages of a dry gas measurement over a 30 hour period (used for estimating CMR). The experiment was performed prior to field deployment.

Fig. C1: please express CH4 in ppb.

Ok.

The spread of intercept looks pretty high (for both CO2 and CH4). Please can you provide the time series of measurement results (expressed as average value of CO2 and CH4) for each single tank during the calibration events?

The spread of the intercept represents the uncertainty for theoretical measurement values of 0 ppm CO2 and 0 ppb CH4. The uncertainty in the range covered by the calibration tanks (and

thus, typical ambient mole fractions) is much smaller and quantified by se_{fit}, which, if computed for individual calibration events, would on average be 0.047 ppm CO2 and 0.11 ppb CH4. For more details, see also the difference between σ_b and $\sigma_{b,min}$ explained in Andrews et al. (2014). The requested plot is shown in Fig. 5 below.

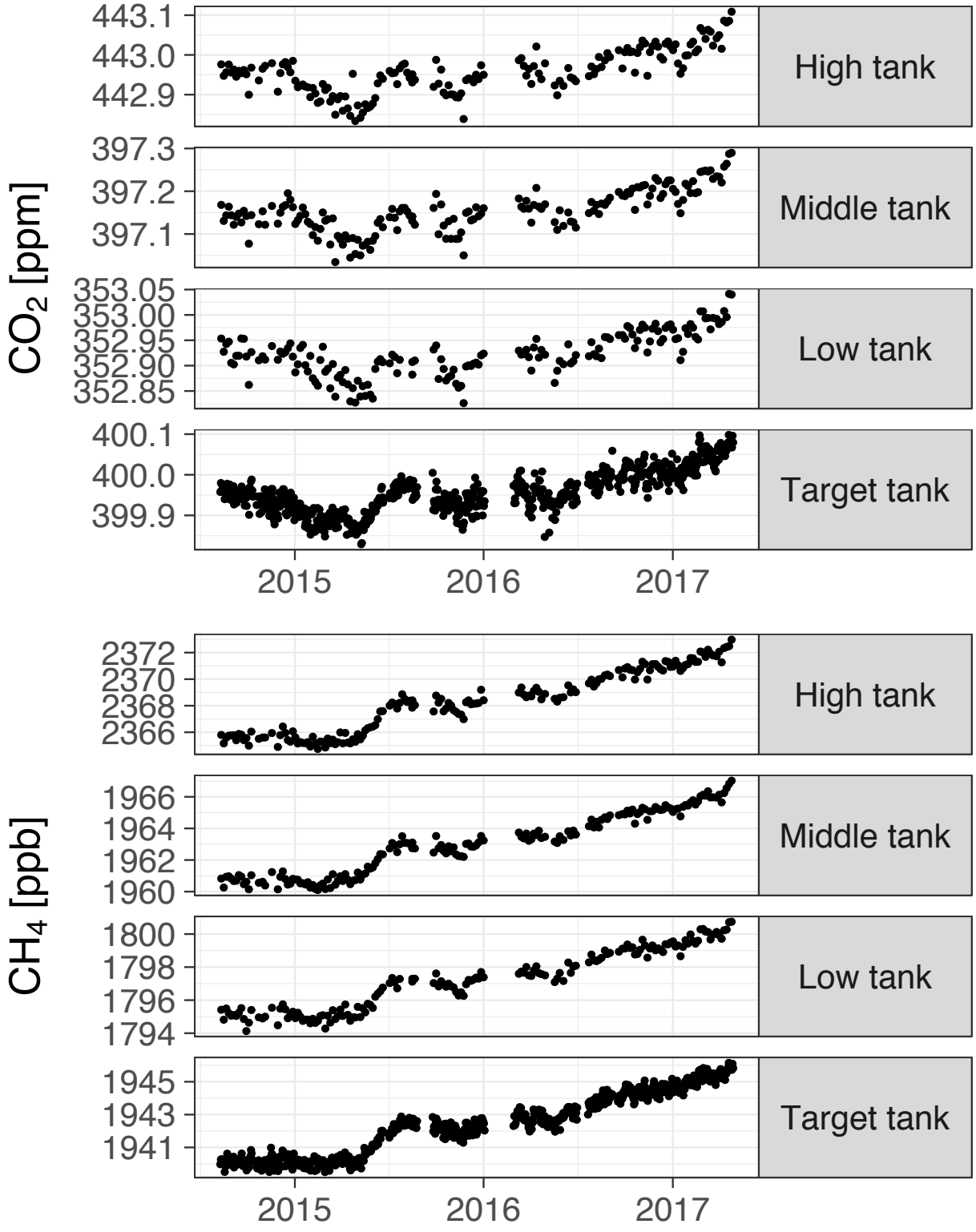

Fig. 5: Timeseries of CO2 and CH4 values from gas tank measurements. Shown here are the last two minutes of each gas tank measurement, i.e. the values that were used to derive calibration coefficients.

Which is the typical value of H2O during the calibration for each tank?

The residual H2O mole fraction is well below 0.01 %. We add this information to the main text.

"3.4 Data screening"

It is not clear if this check are performed automatically or manually. Please provide more details about the screening procedures here adopted (e.g. threshold values, which kind of air pollutants are considered,. . .)

Erroneous measurements (Sect. 3.4.1, 3.4.2, 3.4.4) are removed automatically. For other procedures (listed in Table 1), flagged data are supplied and it is up to the user to use them as they see fit for their application. We clarify this in the introduction to Sect. 3.4. The thresholds given for these parameters were merely examples used in this paper, and it is up to the user to choose thresholds best suited for their application.

-3.4.1 Analyser status diagnostic I'm rather surprised that the OUTLETVALVE parameter is not mentioned in this screening. In my experience this is a pivotal parameters to check the presence of obstruction (e.g. filter) in the system.

We monitor obstructions and other problems based on the flow meters and the pressure sensor in the sampling system. The outlet valve provides redundant information.

-3.4.2 Flushing of the measurement 30 sec is not sufficient as stabilization time. I think that a few minutes is more suitable.

To avoid misunderstandings, the 30 seconds were only used for switching between ambient air inlets. After switching from tanks to ambient air inlets, 5 minutes of flushing were used to account for the much larger differences in CO2, CH4 and H2O mole fractions between gas tank and ambient measurements. We agree with the reviewer that longer flushing of the lines reduces chances of cross-contamination between air sources. However, the purpose of switching between the two inlets is to be able to filter for situations where differences between the two inlets are large. In cases when the differences are large, the timing of trace gas changes when switching between inlets can be observed and is roughly as follows (an example is given in Fig. 6): after ~8 seconds, recorded values start changing rapidly (i.e. this is the residence time between V1 and Picarro cavity). This rapid change lasts for roughly ~10 seconds. Afterwards, changes are small. Certainly not all cross-influence will be removed by then, but since our intention is to detect cases of large differences between the inlets for the purpose of filtering them out, we think that 30 seconds of flushing are sufficient.

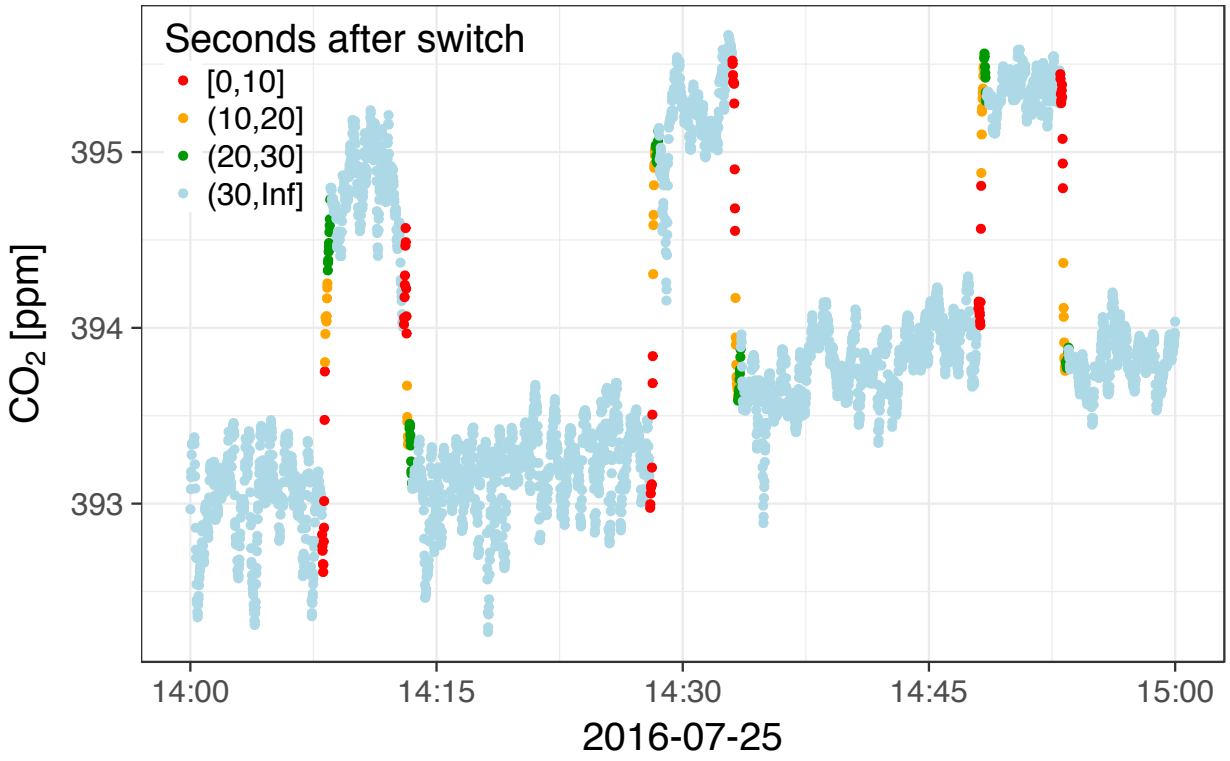

Fig. 6: An example of ambient data of both air inlets illustrating the flushing of the tubing common to both tower inlets. For clarity, we chose an example where differences between the inlets were large compared to the intra-hour variability of each inlet. Colors indicate the time that passed after the inlet was switched by valve V1. Data are used for analysis starting 30 seconds after switching, i.e. the data points in light blue.

-3.4.3 Contamination from local polluters I think that also CH4 need a proper spike detection. What about biological waste management of the base?

We agree that our approach may, in rare cases, lead to CH4 spikes remaining undetected. As described in the manuscript, the major pollutant sources to consider are emissions by the meteorological station itself. Contamination due to waste may be possible in summer only because during other seasons it is mostly frozen. However, the application of the CO2 filter to CH4 data was based on the assessment that, if CH4 spikes were present, they often coincided with CO2 spikes. At the same time, large CO2 spikes are much more frequent than large CH4 spikes at Ambarchik. Thus, given the small impact of the CO2 filter (Table 3 in the manuscript), we think that contamination of the CH4 signal independent from CO2 is a negligible source of bias. Furthermore, every filter based on signal variability is somewhat subjective and bears the risk of removing natural signals. This is particularly problematic in the case of CH4 due to the high variability of its natural emissions. Therefore, we believe that, in case of the Ambarchik station, separate spike detection for CH4 rather holds the potential to reduce the data quality, and we decided that a common filter based on the CO2 time series works best. Note also that CH4 contamination from local sources may be filtered out by other criteria made available to the user. In particular, intra-hour variability is directly affected by potential undetected spikes, and independently provided for CO2 and CH4.

We include these motivations in Sect. 3.4.3 of the revised manuscript.

Table 3: the statistic is referring to all data or the 1-4 PM selection? Looking to Fig. 6, it seems that WD has a strong seasonal variability. How the fraction of flagged data is shared among the different months of the year?

Table 3 refers to all data (we add that to the caption of the table). The annual variation of the impact of the spike filter depends on whether filters are applied (Fig. 7 below).

Here, we present seasonal variations of the fraction of flagged data. We consider the case of applying the temperature gradient ("T") and wind speed ("wv") filter to remove the seasonally varying impact of temperature inversions and wind speed variations. The fraction of affected data follows indeed the wind speed pattern (Fig. 7): more data are affected during the period March–September than October–February. This roughly corresponds to the period when the prevailing wind direction is Northeast, where the inhabited building, and thus contamination sources are located.

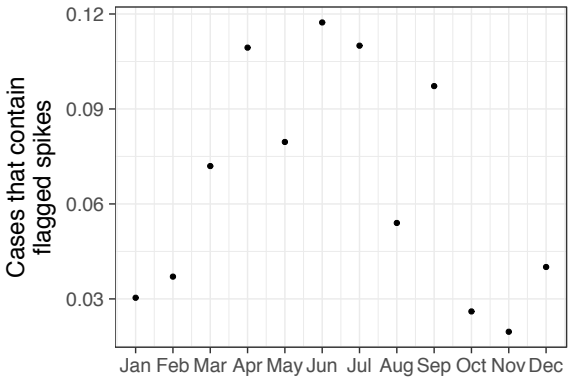

Fig. 7: Fraction of data affected by the CO2 spike flagging. Shown here are data that pass the temperature gradient and wind speed filter from Table 3 of the manuscript.

I would suggest to implement as soon as possible measurements for the monitoring of pollution emissions (CO, NOx or aerosol particle) to consolidate the detection of local pollution influence.

The authors agree with the reviewer that monitoring pollutants continuously would aid the quality control of the greenhouse gas data. Monitoring additional gas species would also significantly enhance the impact of the Ambarchik station for the pan-Arctic GHG monitoring network. Unfortunately, additional continuous sampling is currently not available due to lack of funding. However, we originally planned to extend the observing system in Ambarchik by an ICOS-style automated flask sampler in summer 2019. Due to customs problems, we had to postpone this installation until summer 2020. Drawing air samples at regular intervals, but also considering the targeted sampling of specific emission events, including spikes, this new data source will allow in-depth interpretations of the existing, continuous monitoring program presented within this manuscript.

"Section 5.1."

Line 12. Please do not use "trend" for this short time period. Use "tendencies" or (when appropriate) "growth rate" (the same for CH4)

We replace the term “trend” by “average growth rate over the analyzed period”.

Line 26: more than this “trend” along the whole measurement period, a discussion of the annual growth rates could be more interesting.

We attempted to quantify annual growth rates based on averaging springtime measurements, but the results depended on the averaging period. The curve fitting procedure applied here, consisting of 4 harmonics plus a linear trend, may also be used to infer annual growth rates, but in light of the short data coverage period, the present analysis was chosen because it appeared most robust.

I do not agree that the attribution of the very high values of CO2 in December 2016 are outside the scope of the paper. They can indicate analytical/experimental problems or interesting phenomena can be investigated at the station. I strongly suggest to provide some sounding explanations.

We are highly confident that this signal is not due to measurement errors, because it was also observed by the gas analyzers of an eddy-covariance station operated by MPI-BGC near Chersky, approximately 100 km to the south of Ambarchik. Even though these analyzers (LosGatos FGGR) are not as well calibrated as the Picarro instrument at Ambarchik, their data quality is clearly good enough to observe such a pronounced signal.

At the same time, it is obvious that the detailed interpretation of such a signal, including an attribution to specific emission processes and/or source regions, would require an extended analysis that is clearly beyond the scope of the presented paper. With the signal being detected also at other sites, it is clear that we either see a large-scale anomaly in surface-to-atmosphere emissions, or the effect of an unusual atmospheric transport pattern. To differentiate between both, data from many more sites within the Arctic domain would be required, including also a reliable dataset on the variability of the background signal entering this domain. All of this must therefore be referred to a follow-up paper.

"Section 5.2"

This section is really basic. The related goal is not clear to me as well as the method for deriving the background values of CO2 and CH4. Please explain better. No explanation or discussion are provided for the results from wind analysis in section 5.2.1 and 5.2.2.

The analyses shown in Section 5.2 provide hints on source/sink regions for the signals detected at Ambarchik. This is of particular interest at Ambarchik because it is located at a junction of several different ecoregions (e.g. land/ocean). Thus, to first order, we expect that differences in the signals by wind direction hint at differences between these regions. To clarify our intention, we add this motivation to Sect. 5.2. The results demonstrate that there is indeed an angular dependence in the observations that hint at terrestrial regions, as opposed to the ocean, as the dominant contributor to regional CO2 and CH4 anomalies captured at Ambarchik. This demonstrates the value of sampling at this location for insights into regional carbon cycle processes. We add this consideration to the conclusions section.

Our computation of background values follows a standard method in regional inverse modeling of atmospheric tracer transport, meaning that the background corresponds to the contribution of

CO2/CH4 transported into the examined domain. By subtracting this signal from the observations, only the signature of sources and sinks inside the domain remains. We reformulate the section to clarify this procedure.

A conclusion drawn from results presented in Sect. 5.2 was already given in Sect. 6, i.e. that larger CO2 and CH4 signals appear to be of terrestrial rather than oceanic origin. In the revised manuscript, we slightly expand this by highlighting the added value of the unique station location as a reference to the newly added motivation of Sect. 5.2.

"Section 6"

Line 14. I do not think that the WMO compatibility goal and your total uncertainty can be directly compared. Instead, the “compatibility goal” is not (better: may not be) your achievable total uncertainty but a specific value within which your measurements must agree (see GAW Report No. 206).

Correct. We delete the sentence in question.

Author's response to review 2

The paper describes a unique and valuable dataset collected in a harsh environment in an under-sampled region. These data will be valuable for inverse modeling to estimate emissions and removals of CO2 and CH4. Arctic data such as these are particularly needed, since release of carbon from permafrost is an expected outcome from warming temperatures and current estimates of Arctic fluxes vary widely. The authors provide a useful and complete description of challenges of operating in the Arctic and their strategies for maintaining continuous operations and filtering data to remove local effects. The description of the configuration is comprehensive and clear. The authors have provided quantitative and time-varying uncertainty estimates and a clear description of how the uncertainty was estimated.

A concern is that the data is available "on request" rather than readily available for download (e.g. from the WMO Global Atmosphere Watch World Data Center for Greenhouse Gases or these data could be included in the GLOBALVIEW+ ObsPack product compiled by NOAA). The value of these data will only be realized when combined with other datasets from the global community.

We agree with the reviewer that the value of our dataset for the atmospheric research community will be substantially increased by making the data 'visible' in one of the commonly used online repositories. A publication of these datasets in a public and visible repository (e.g. WDCGG) is therefore foreseen for the near future.

Also, the spike detection algorithm seems to be highly tuned and somewhat arbitrary (but to be fair data from many sites are manually flagged, which relies on expert judgment that is arguably even more arbitrary). Please see specific comments about making the flagging criteria explicitly available so that users have enough information to develop their own filtering scheme.

All criteria and thresholds used for the spike detection were given in detail in Appendix D, which should enable reproducing the procedure. Since the chosen settings were customized for Ambarchik, we agree with the reviewer that an adaptation of this method at other sites would require an adaptation of these criteria. Still, we believe that we presented an objective method to remove spikes that both clearly demonstrates how we filtered our own data, and moreover should be applicable also to other datasets, given that the PIs are willing to fine-tune the settings.

~~~~~~~~~~~~~~~~~~~~~~~~~~~~~~ Review Criteria for AMT: ~~~~~~~~~~~~~~~~~~~~~~~~~~~~~~

Does the paper address relevant scientific questions within the scope of AMT? yes

Does the paper present novel concepts, ideas, tools, or data?yes the data from this new Arctic site are novel and uniquely valuable for tracking possible release of CO2 or CH4 from permafrost

Are substantial conclusions reached?yes in the sense that 2+ years of data are presented along with an assessment of enhancements over background presented versus wind direction and season

Are the scientific methods and assumptions valid and clearly outlined?yes
~~~~~~~~~~~~~~~~~~~~~~~~~~~~~~

Are the results sufficient to support the interpretations and conclusions?yes

Is the description of experiments and calculations sufficiently complete and precise to allow their reproduction by fellow scientists (traceability of results)? yes with some minor requests for clarification below

Do the authors give proper credit to related work and clearly indicate their own new/original contribution?yes

Does the title clearly reflect the contents of the paper?yes

Does the abstract provide a concise and complete summary?yes

Is the overall presentation well structured and clear?yes

Is the language fluent and precise?yes

Are mathematical formulae, symbols, abbreviations, and units correctly defined and used?yes

Should any parts of the paper (text, formulae, figures, tables) be clarified, reduced, combined, or eliminated?no, the paper is of appropriate length and detail

Are the number and quality of references appropriate?yes

Is the amount and quality of supplementary material appropriate?yes

We thank the reviewer for this very positive evaluation of our manuscript in light of the AMT review criteria.

~~~~~~~~~~~~~~~~~~~~~~~~~~~~~~~~ Specific Comments: ~~~~~~~~~~~~~~~~~~~~~~~~~~~~~~~~

page 6 what is the flow rate through the analyzer and what is the purge flow rate?

The nominal flow rate in the sample line (as measured by FM2) is ~170 mL/min. We add this information to Sect. 2.3. The purge flow (FM1) is ~17 L/min and was already reported in Sect. 2.3.

page 9, line 25: Is there any indication if the time synching with the GPS fails?

Time synchronization takes place between GPS clock and Picarro clock, and separately between Picarro clock and data logger clock. The latter synchronizations are protocolled and can thus be checked. However, this is usually not done, since so far there was no indication that there were timing issues.

page 10 line 20: State that "synthesis" function is defined in Appendix B.

We add this reference there.
~~~~~~~~~~~~~~~~~~~~~~~~~~~~~~~~

page 10 lin3 16: Variability of water correction experiments discussed by Stavert et al., AMTD, 2018 (https://www.atmos-meas-tech-discuss.net/amt-2018-140/) and could be referenced here. They found that short-term repeatability of water corrections was similar to long-term repeatability.

This could indeed be an indication that we observe short-term variations. We add this information to the text.

page 12: what is the expected lifetime of each calibration cylinder?

The Target tank was replaced in summer 2018 and thus lasted 4 years. At this rate, regular calibrations would deplete the calibration cylinders in 16–24 years. However, these tanks are also used for other experiments like water corrections and are thus depleted far more rapidly. They are currently 40-50% depleted (status: February 2019, i.e. after 4.5 years of operation).

page 13: it would be useful to describe the stochastic and non-random components of the estimated measurement uncertainty (i.e. to what extent does the uncertainty improve with averaging).

This topic is mentioned again in another comment below, where we address it.

The text states that the uncertainty is dominated by the water correction, which is not going to improve with averaging. But perhaps also include a statement about the short-term precision of the analyzer for each gas (i.e. what is the standard deviation on each 10-minute calibration after the gas has equilibrated).

We discussed short-term precisions in the response to review 1, and discuss random and systematic uncertainty components in the response to the review comment about page 32 below.

What is the typical standard error of the residuals?

The standard errors of individual calibration events were 0.018 ppm CO2 and 0.04 ppb CH4.

page 16: description of data filtering algorithms is useful and the results shown in Table 3 demonstrate that impact is practically negligible.

Ok.

page 16: description of water vapor spikes is interesting, and the explanation seems plausible

Ok.

page 17: it would be useful to see how the virtual potential temperature threshold corresponds to other indicators of difficult-to-model observations. For example, are hourly standard deviations typically higher than during well-mixed conditions? What is the duration of a typical inversion (i.e. how many consecutive hours of data are typically flagged)? Can these events be reliably screened based on something like enhancement above a smoothed background? This type of information could be helpful for developing filters for other sites (particularly Arctic sites) where virtual potential temperature information is lacking.

We agree that our data might be useful for developing filters for other sites. However, it would not be guaranteed that relationships between filter criteria in Ambarchik would be valid universally. Transferable relationships would have to be validated with analogous data from other sites. This is beyond the scope of this paper, but could be done with the data we distribute. This may be an interesting topic for a follow-up paper. For this paper, however, such an extended analysis is beyond the scope we set up, so we decided to not follow up on these remarks.

page 18, line 5: what is the duration of the back trajectories (i.e how many hours or days backward in time)?

We used 15-day backtrajectories for these analyses. We add this information to the text.

page 20, line 6: How are Barrow data selected for this comparison. State clearly that you are including Barrow data that has not received a first column flag if that is the case.

Correct, that was essentially the quality filter. We add the following explanatory paragraph to the text:

Barrow data were filtered according to their quality flag. For CO_2, data with quality flags "...", ".D.", ".V." and ".S." were included. For CH_4, data with quality flags "..." and ".C." were included. Data with other flags than a "." in the first column were removed as invalid. Other quality flags (differing in the second or third column) were excluded because their number was negligible.

Can you speculate about why the virtual potential temperature filter would remove such a large fraction of the data at Barrow? Is there some obvious difference in the meteorological conditions at the two sites? Does this result have implications for interpreting the Barrow data?

First, we calculated the intercomparison between Ambarchik and Barrow also without the temperature filter for Ambarchik data, and resulting plots look virtually identical. Accordingly, this filter is not essential for the site intercomparison presented in the manuscript.

As we see it, the differences in the wintertime near-surface temperature profiles between both sites can most likely be related to the surface structure in the near field of the stations, rather than to differences in climate. With Ambarchik being situated close to the shoreline of the Arctic Ocean, on top of a low cliff, the level of mechanically generated turbulence is comparatively high. The Barrow station, on the other hand, is situated in very flat terrain, so that mechanically generated turbulence is less likely to break up stable stratification of near-surface air masses. Thus, temperature inversions might occur less frequently in Ambarchik than in Barrow. Since these considerations are speculative, we do not include them in the manuscript.

page 15: regarding amplitude estimation, maybe it would be better to use the curve including residuals and then estimate the amplitude based on the difference between the min max smooth curve values (and you could just compute the average for all the consecutive min-max or max-min pairs). Then you could do same with to ensure apples to apples comparison. Otherwise when you compare Barrow and Ambarchik are the amplitudes different because of different time periods?

The time periods for estimating the amplitudes for Ambarchik and Barrow were identical, as depicted in the plots. We agree with the reviewer that the min/max fitting outlined by him/her may provide additional information that may become helpful when applying this procedure in other contexts. However, in the case of the data presented herein, we do not believe that this alternative way of computing the amplitudes would add information that would change our data interpretation. We will therefore not change the approach presented here.

page 20, line 22: are you sure that the smaller variability at Barrow was real and not due to differences in screening for the two sites?

Yes, since we used virtually all data at Barrow (see above).

page 22: Were the trajectory endpoints the actual endpoints for the entire Arctic WRF domain? Or did you define a subdomain? It would be useful to provide some information about the locations of the endpoints (such as vertical and lat lon distributions by season or for some typical examples).

We used the domain introduced in Sect. 4 (3200 km x 3200 km). Most trajectories leave this domain, but in case a trajectory did not, its endpoint was sampled within the domain. In Fig. 1, we show the distribution of trajectory end points and their height above ground level for all simulated trajectories. However, we think that this is too much detail for the paper and therefore will not include these figures there.

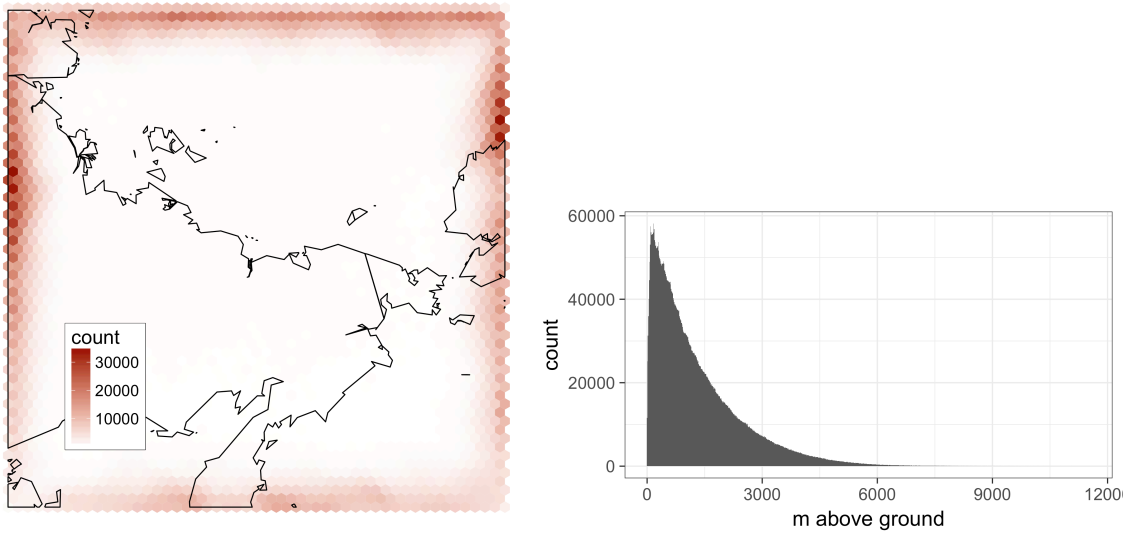

Fig. 1: Spatial distribution of trajectory endpoints for Ambarchik in the domain used in this paper. Left: geographical distribution. Right: height above ground level.

page 24 line 16: instead of "exceeded the goal" perhaps say "did not meet the goal" (although I am not sure the uncertainty estimate is accurate to 0.01 ppm, so maybe you could say instead something like "meeting the goal to within our ability to estimate the uncertainty). Certainly you are doing as well as any other group in the world, and better than most at documenting the uncertainties.

We delete this sentence because, as pointed out by reviewer 1, the values are not directly

comparable.

page 29, line 6: differences among sequential individual co2 measurements?

Yes. We add ‘consecutive’ to this sentence, so that it reads: “Candidates for CO2 spikes are identified based on the variability of differences between consecutive CO2 measurements.”

page 29, line 11: it’s not clear how "cases when all CO2 data in the interval have rather uniform variations" are identified so that they can be unflagged

We clarify by replacing this sentence with the following paragraph:

In some cases, this procedure flags the complete interval as spikes. This happens when the variations throughout the interval are rather uniform. This might be the case both in the presence of spikes throughout the interval, or absence of spikes altogether. To avoid false positives, all flags are removed, and the interval is considered to have no spikes. Cases with many spikes throughout the interval can be filtered based on the intra-hour variability flag.

page 29, step 3: why is it not desirable to also flag short-duration spikes? Couldn’t these originate from a very local source, such as a generator?

This unflagging step concerns data points that we consider statistical outliers. Since step 1 features a variability threshold of 3.5 standard deviations, it flags data points with natural variation. Assuming a Gaussian distribution of the variability and no spikes, 0.05 % of all valid data points would be expected to exceed the threshold of 3.5 standard deviations. Therefore, we consider individual flagged data points, or very small groups thereof, false positives. Therefore, they are unflagged in step 3. In addition to the above reasons, their impact is negligible and they would complicate further steps, which is why they are unflagged in step 3.

page 30, line 2: why choose a threshold of 8 std deviations? this seems arbitrary

All parameters in the spike detection algorithm were tuned to work with the data from Ambarchik, so might seem arbitrary. We do not claim that these settings can be applied to different sites without further review. The chosen criteria worked best for our own site, and we believe they may also provide good starting values in case the procedure is applied to other datasets.

page 31, Figure D.1: This figure shows the utility of using an algorithm to remove spikes and it does seem to work reasonably well for this case. But the complexity of the strategy is concerning. When the data is distributed, it would be best if the flagging for spike-detection is reported separately from other types of flagging (e.g. flagging after transitions, flagging for maintenance) so that the end user can consider alternative strategies.

We fully agree with the reviewer on this topic. Because of the complexity of the algorithm, we distribute hourly data both with and without application of the spike detection algorithm. Note, however, that the impact of the algorithm on atmospheric data was small anyway (see Table 3 in the manuscript).

page 32, E.1 It would be useful to describe the Allan variance of the analyzer and to distinguish

between random error that reduces with averaging versus uncertainties that result from systematic errors that cannot be reduced by averaging.

We add a description of random and systematic uncertainty components together with Allan deviation plots as new section Appendix E.3. To summarize, our error model relies on the following components: uncertainty due the calibration strategy, uncertainty of the water correction, instrument drift and noise. Of these uncertainties, only instrument drift and noise (σ_u, σ_y') are affected by averaging. For a better understanding of this component, we computed the Allan deviation based on the 12-day calibration measurement that was used for estimating σ_u (see revised manuscript). The results (Fig. 2, also included in the revised manuscript) indicate that further averaging does not improve the uncertainty due to the random components, i.e. instrument noise and drift. The Allan deviation estimates of our analyzer are within the range of those for several gas analyzers of the same type as ours, as documented in Yver Kwok et al. (2015).

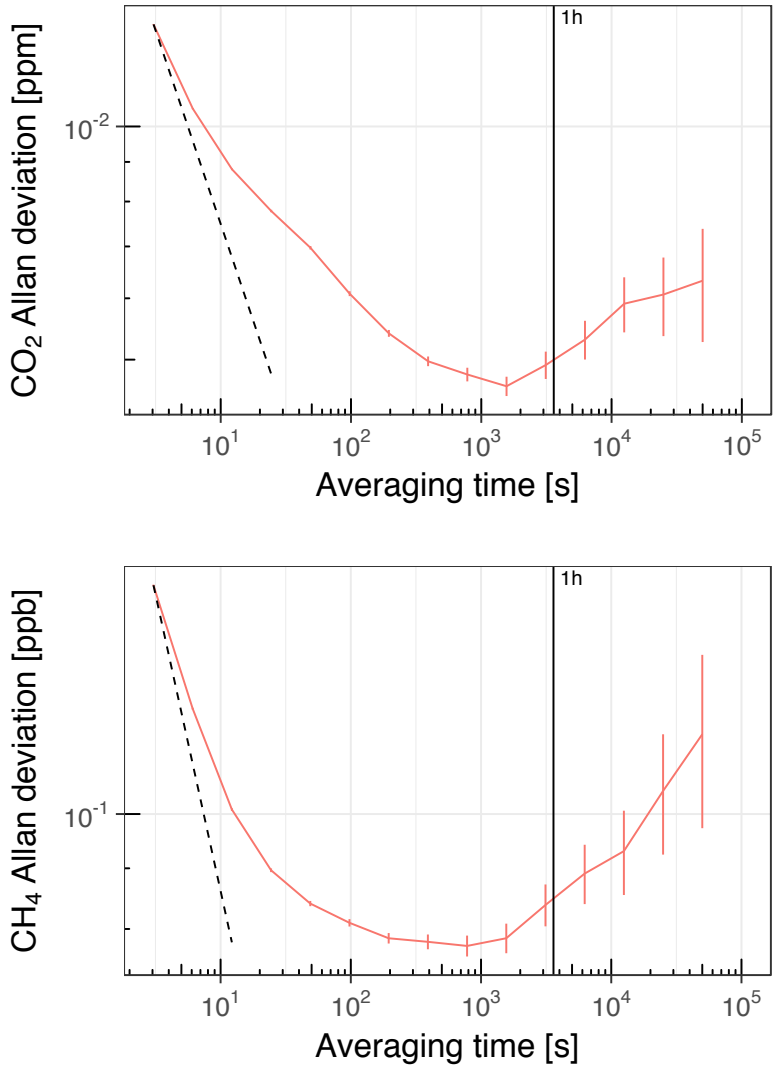

Fig. 2: Allan deviation of the CO2 and CH4 readings of the CRDS analyzer in Ambarchik. Values are based on one 12-day measurement of dry air from a gas tank in the lab prior to field deployment. The averaging time is cut off where the error gets too large for a meaningful interpretation of the result. The vertical line denotes an averaging

time of one hour. The dashed line corresponds to white noise (slope -0.5), scaled to coincide with the first data point of the Allan deviation.

Specifically, if laboratory tests or field calibration data can be used to estimate the random component at the native frequency of the measurement and for hourly averages, then that would allow the user to determine when atmospheric variability exceeds the random noise of the Picarro analyzer. This can help with data selection and weighting in inverse modeling. See the discussion of "sensor precision and atmospheric variability" in the recently released GGMT 2017 meeting report (GAW Report 242).

The analyzer signal drift and precision for hourly averages was reported in Appendix E as σ_u. The values were: 0.013 ppm CO2, 0.25 ppb CH4. We add these values, and a statement that they might be used to distinguish between analyzer signal and atmospheric variability, to Sect. 3.4 "Uncertainty in CO2 and CH4 measurements".

A related question is whether the standard error of the fit takes into account the 120 day smoothing of the coefficients. For a simple case with a uniform (boxcar) 120 day weighting, there would be approximately 24 separate calibration episodes = 70 degrees of freedom. The standard error is substantially reduced compared to a single calibration episode. An example with realistic values and errors is given in the attachment (coded in R) and improvement in the fit coef uncertainties and the overall residual standard error of the fit is evident when multiple calibrations are combined. Here I neglected noise on the assigned values. It should be straightforward to adapt the equations from Andrews et al., 2014 Appendix D to account for the tricubic kernel weighting if that method is demonstrably superior to simple boxcar smoothing.

We thank the reviewer for spotting this error in our analysis! Indeed, our uncertainties did not account for the error reduction achieved by smoothing the coefficients – which was of course the purpose of the smoothing. We update our analysis by calculating new calibration fit functions, this time based on using all calibration episodes in the averaging window and with the weights used for averaging coefficients. We confirmed that our averaged coefficients were virtually identical to those based on these weighted fits, and did therefore not change them. We then recomputed the uncertainty components that were affected. Below, we summarize which terms were affected how by this correction:

$z_{(\alpha,f)}$: Reduced because of the increased degrees of freedom (~1 now).

σ'_y: Increased for CH4 because residuals now correctly account for instrument drift. For CO2, the values decreased because the residuals were typically larger than the drift.

se_{fit}: Competing effects of reduction due to the larger number of observations and increase because of instrument drift.

Also, we previously reported $z_{(\alpha,f)}\sigma'_y$ and $z_{(\alpha,f)}se_{fit}$ in Table E.1, instead of σ'_y and se_{fit}. This was supposed to give a better sense of the contribution of these quantities to the total error. However, since this fact was omitted in the manuscript, and $z_{(\alpha,f)}$ is roughly equal to 1 now, we switch to reporting σ'_y and se_{fit} as stated in the table.

The standard error of the fit (se_{fit}) is now computed based on the equations given in Andrews et al. (2014), but modified for the case with varying weights (following Taylor, 1997).

We update the description of the uncertainty estimation in Appendix E.1, including the formulas for the uncertainty components for fits with weights, the values of the affected components in Table E.1 and the final uncertainty estimates in Fig. E.1.

Note that instrument drift now affects both se_{fit} and σ_u. However, while se_{fit} captures drift on the time scale of the averaging window of 120 days, it treats drift significantly below this time scale as noise. Thus, the contribution of drift on these shorter timescales to se_{fit}would tend toward 0 for larger numbers of measurements. By contrast, our estimate of σ_u is based on measurements over the significantly shorter period of 12 days. Therefore, it serves as an estimate of short-term drift not captured by the smoothed calibration coefficients, and is left unchanged.

And/or you could use the "residual standard error" of the fit to find the optimal averaging window and weighting strategy.

This would indeed provide an interesting study objective. However, it is outside the scope of the presented manuscript, and therefore needs to be postponed to a follow-up study.

The "sigma prime y" term in E.4 will also be affected by analyzer noise, and may be smaller for an hourly average value than for a single calibration episode. In any case, it is important to describe the random error characteristics of the analyzer and the individual calibration episodes.

As described above, we add a section on “Random and systematic uncertainty components” to the appendix (Appendix E.3), where we discuss these considerations. In short, random uncertainty components only played a minor role in our uncertainty estimates.

Please also note the supplement to this comment: https://www.atmos-meas-tech-discuss.net/amt-2018-325/amt-2018-325-RC2- supplement.pdf

Accurate measurements of atmospheric carbon dioxide and methane mole fractions at the Siberian coastal site Ambarchik

Friedemann Reum[1], Mathias Göckede[1], Jost V. Lavric[1], Olaf Kolle[1], Sergey Zimov[2], Nikita Zimov[2], Martijn Pallandt[1] and Martin Heimann[1, 3]

[1]Max Planck Institute for Biogeochemistry, Jena, Germany
[2]North-East Science Station, Pacific Institute for Geography, Far-Eastern Branch of Russian Academy of Science, Chersky, Republic of Sakha (Yakutia), Russia
[3]University of Helsinki, Faculty of Science, Institute for Atmospheric and Earth System Research (INAR) / Physics, Finland

Correspondence to: Friedemann Reum (freum@bgc-jena.mpg.de)

Abstract. Sparse data coverage in the Arctic hampers our understanding of its carbon cycle dynamics and our predictions of the fate of its vast carbon reservoirs in a changing climate. In this paper, we present accurate measurements of atmospheric CO_2 and CH_4 dry air mole fractions at the new atmospheric carbon observation station Ambarchik, which closes a large gap in the atmospheric trace gas monitoring network in northeastern Siberia. The site, operational since August 2014, is located near the delta of the Kolyma River at the coast of the Arctic Ocean. Data quality control of CO_2 and CH_4 measurements includes frequent calibrations traced to WMO scales, employment of a novel water vapor correction, an algorithm to detect influence of local polluters, and meteorological measurements that enable data selection. The available CO_2 and CH_4 record was characterized in comparison with in situ data from Barrow, Alaska. A footprint analysis reveals that the station is sensitive to signals from the East Siberian Sea, as well as northeast Siberian tundra and taiga regions. This makes data from Ambarchik highly valuable for inverse modeling studies aimed at constraining carbon budgets within the pan-Arctic domain, as well as for regional studies focusing on Siberia and the adjacent shelf areas of the Arctic Ocean.

1 Introduction

Detailed information on the distribution of sources and sinks of the atmospheric greenhouse gases (GHG) CO_2 and CH_4 is a prerequisite for analyzing and understanding the role of the carbon cycle within the context of global climate change. The Arctic plays a unique role in the carbon cycle because it hosts large carbon reservoirs preserved by cold climate conditions (Hugelius et al., 2014; James et al., 2016; Schuur et al., 2015). Yet, the net budgets of both terrestrial (Belshe et al., 2013; McGuire et al., 2012) and oceanic (Berchet et al., 2016; Shakhova et al., 2014; Thornton et al., 2016) carbon surface-atmosphere fluxes are still highly uncertain, as are the mechanisms controlling them. Furthermore, the Arctic is subject to faster warming than the global average at present and in the coming decades (IPCC, 2013). Thus, a considerable fraction of terrestrial (Schuur et al., 2013) and subsea (James et al., 2016) permafrost carbon reservoirs is at risk of being degraded and released under future climate change. The fate of further carbon reservoirs in the Arctic seabed is uncertain as well under warmer conditions. A substantial release of the stored carbon in the form of CO_2 and CH_4 would constitute a significant positive feedback enhancing global warming. Therefore, improved insight into the mechanisms that govern the sustainability of Arctic carbon reservoirs is essential for the assessment of Arctic carbon-climate feedbacks and the simulation of accurate future climate trajectories.

A key limitation for understanding the carbon cycle in the Arctic is limited data coverage in space and time (Oechel et al., 2014; Zona et al., 2016). Besides infrastructure limitations, the establishment of long-term, continuous and high-quality measurement programs at high latitudes is severely challenged by the harsh climatic conditions especially in the cold season (Goodrich et al., 2016). During the Arctic winter, even rugged instrumentation may fall outside its range of applicability, and measures may be required to prevent ice buildup and instrument failure without compromising data quality (Kittler et al., 2017a). Also, many sites are difficult to access for large parts of the year, complicating regular maintenance and therefore increasing the risk of data gaps because of broken or malfunctioning equipment.

A widely used approach to quantify carbon fluxes on a regional scale builds on measurements of atmospheric CO_2 and CH_4 mole fractions and inverse modeling of their transport in the atmosphere (Miller et al., 2014; Peters et al., 2010; Rödenbeck et al., 2003; Thompson et al., 2017). The

performance of inverse models to constrain surface-atmosphere exchange processes depends on the accuracy of atmospheric trace gas measurements. Because biases in the measurements (e.g. drift in time or bias between stations) translate into biases in the retrieved fluxes (Masarie et al., 2011; Peters et al., 2010; Rödenbeck et al., 2006), the World Meteorological Organization (WMO) has set requirements for the inter-laboratory compatibility of atmospheric measurements: ±0.1 ppm for CO_2 in the northern hemisphere and ±0.05 ppm in the southern hemisphere, and ±2 ppb for CH_4 (WMO, 2016).

Atmospheric inverse modeling has a high potential for providing insights into regional to pan-Arctic scale patterns of CO_2 and CH_4 fluxes, as well as their seasonal and interannual variability and long-term trends. The technique could also serve as a link between smaller scale, process-oriented studies based e.g. on eddy-covariance towers (Euskirchen et al., 2012; Kittler et al., 2016; Zona et al., 2016) or flux chambers (e.g. Kwon et al., 2017; Mastepanov et al., 2013) and the coarser scale satellite-based remote sensing retrievals of Arctic ecosystems and carbon fluxes (e.g. Park et al., 2016). However, to date, sparse data coverage limits the spatiotemporal resolution and the accuracy of inverse modeling products at high northern latitudes. To improve inverse model estimates of high latitude GHG surface-atmosphere exchange processes, the existing atmospheric carbon monitoring network (Fig. 1) needs to be expanded (McGuire et al., 2012).

In this paper, we present the new atmospheric carbon observation station Ambarchik, which improves data coverage in the Arctic. The site is located in northeast Siberia at the mouth of the Kolyma River (69.62° N, 162.30° E) and is operational since August 2014. In Sect. 2, we introduce the station location and instrumentation, and in Sect. 3 the quality control of the data. We characterize which areas the station is sensitive to in Sect. 4, and present a signal characterization of the available record in Sect. 5. Section 6 contains concluding remarks.

Revision 2.9.2019 11:07

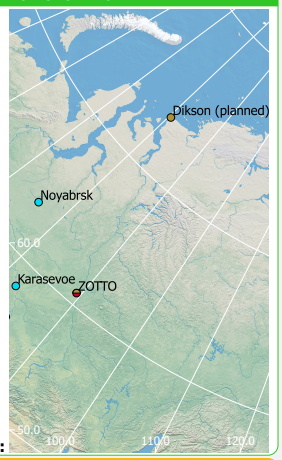

Gelöscht:

Unknown

Formatiert: Schriftart:9 pt

Fig. 1: Stations observing atmospheric CO_2 and CH_4 in Northeast Siberia (including Barrow, Alaska). At all stations but Yakutsk, continuous in situ monitoring takes place. In Yakutsk, flasks are sampled monthly onboard an aircraft. In Tiksi and Barrow, flasks are sampled by NOAA in addition to the continuous in situ measurements.

2 Station description

2.1 Area overview

Ambarchik is located at the mouth of the Kolyma River, which opens to the East Siberian Sea (69.62° N, 162.30° E; Fig. 2). The majority of the landscape in the immediate vicinity of the locality is wet tussock tundra. On ecoregion scale, Ambarchik is bordered by Northeast Siberian Coastal Tundra ecoregion in the West, the Chukchi Peninsula Tundra ecoregion in the East, and the Northeast Siberian Taiga ecoregion in the South (ecoregion definitions from Olson et al., 2001). Major components contributing to the net carbon exchange processes in the area are tundra landscapes including wetlands and lakes, as well as the Kolyma River and the East Siberian Arctic Shelf.

Fig. 2: Ambarchik station location. Background based on Copernicus Sentinel data from 2016.

2.2 Site overview

Ambarchik hosts a weather station operated by the Russian meteorological service (Roshydromet), whose staff is the entire permanent population of the locality. The closest town is Chersky (~100 km to the south, population 2,857 as of 2010), with no other larger permanent settlement closer than 240 km. The site therefore does not have any major sources of anthropogenic greenhouse gas emissions in the near field. The only regular anthropogenic CO_2 and potentially CH_4 sources that may influence the measurements are from the Roshydromet facility, including the building that hosts the power generator and the inhabited building.

The atmospheric carbon observation station Ambarchik started operation in August 2014. It consists of a 27 m-tall tower with two air inlets and meteorological measurements, while the majority of the instrumentation is hosted in a rack inside a building. The rack is equipped for temperature control, but due to the risk of overheating, it is open most of the time and thus in equilibrium with room temperature (room and rack temperature are monitored). Atmospheric mole fractions of CH_4, CO_2, and H_2O are measured by an analyzer based on the cavity ring-down spectroscopy (CRDS) technique (G2301, Picarro Inc.), which is calibrated against WMO-traceable reference gases at regular intervals (Sect. 3.2).

The tower is located 260 m from the shoreline, with a base elevation of 20 m a.s.l. (estimated based on GEBCO_2014 (Weatherall et al., 2015), which in this region is based on GMTED2010 (Danielson and Gesch, 2011)).

2.3 Gas handling

The measurement system allows switching between two different air inlets and four different calibration gas tanks (Fig. 3). Component manufacturers and models of the individual components are listed in Table A.1.

Air inlets with rain guards are mounted on the tower at 27 ("Top") and 14 ("Center") m a.g.l., respectively, and are equipped with 5 µm polyester filters (labels F1 and F2 in Fig. 3). The two air inlets are probed in turns (15 minutes Top, 5 minutes Center). Signals from the Center Inlet are mainly used for quality control purposes (Sect. 3.4). Air is drawn from the inlets (I1, I2) through lines of flexible tubing (6.35 mm outer diameter) by a piston pump located downstream of the measurement line branch (PP1). The cycles of the pump are smoothed by a buffer with a volume of about 5 liters. The combined flow through both inlet lines is about 17 l/min, monitored by a flow meter (FM1) and limited by a needle valve (NV1). The tubing enters the house at a distance of about 15 m from the tower. The air passes 40 µm stainless steel filters (F3, F4), behind which the sample line is branched from the high flow line. A solenoid valve (V1) is used to select between the two inlets.

The sample line (between filters F3/F4 and the CRDS analyzer) is composed exclusively of components made of stainless steel; they include tubing (SS tube 1/8"), two 2 µm filters (F5, F6), a needle valve for sample flow regulation (NV2, usually fully open), a pressure sensor (P1), and a flow meter (FM2). Air is drawn from the high flow line into the sample line by a membrane pump downstream of the CRDS analyzer (MP1). The nominal flow rate in the sample line is 170 mL min^{-1}. The residence time of sample air in the tubing between inlets and CRDS analyzer is on the order of 12 seconds.

Calibration gases pass through a line composed exclusively of stainless steel components as well. Air from gas tanks (High, Middle, Low, Target) passes through pressure regulators (RE1–4), reducing their pressure roughly to ambient pressure. This way, the CRDS analyzer can cope with the pressure difference between sample air and calibration air from the tanks without an open split, which would

Revision 2.9.2019 11:07
Gelöscht: using a

Revision 2.9.2019 11:07
Gelöscht:).

normally be installed to equilibrate the line with ambient pressure. This setup was chosen in order to conserve calibration air. The lines from the gas tanks are connected to a multiposition valve (MPV1), which is used to select between gas tanks. Downstream of the multiposition valve, the calibration gas line is connected to the sample line by a solenoid valve (V3). The solenoid valves V2 and V3 are used to select between sample air from the tower and calibration air.

During calibrations, the part of the measurement line that is not part of the calibration line is continuously flushed by the high flow pump (PP1) through the purge line, which comprises solenoid valve V4 (which shuts off air flow from the gas tanks through the purge line in case of a power outage during a tank measurement), needle valve NV3 (which is used to match the purge flow to the usual sample flow), and flow meter FM3 (which monitors the purge flow).

The flow meters (FM1–3) and pressure sensor (P1) are used to diagnose problems such as weakening pump performance, clogged filters, leaks or obstructions.

The gas handling system was tested for leaks after installation. This was done by capping the tubing and evacuating it using a hand pump to pressures of 0.3–0.4 bar (normal operating pressure is around 0.7 bar). The leak rate was then computed from pressure increase over several hours, corrected for temperature fluctuations measured in the lab. To mitigate the effect of inhomogeneous temperature fluctuations throughout the tubing and increase sensitivity of the pressure to small leaks, the experiments were limited to the small tubing volume inside the laboratory, ignoring the tubing on the tower. This is the part that is most susceptible to leaks, due to the number of tubing connections and the potentially higher CO_2 mole fractions. The results of several such experiments indicated leak rates on the order of no more than 1.3×10^{-6} mbar L s^{-1}. At this rate, CO_2 and CH_4 contamination is negligible even with extremely high mole fractions in the laboratory. During later maintenance visits, simpler leak tests, which did not require opening tubing connections, were performed by breathing on individual connectors and observing the CO_2 mole fraction measured by the gas analyzer. No indications of leaks were observed during these tests.

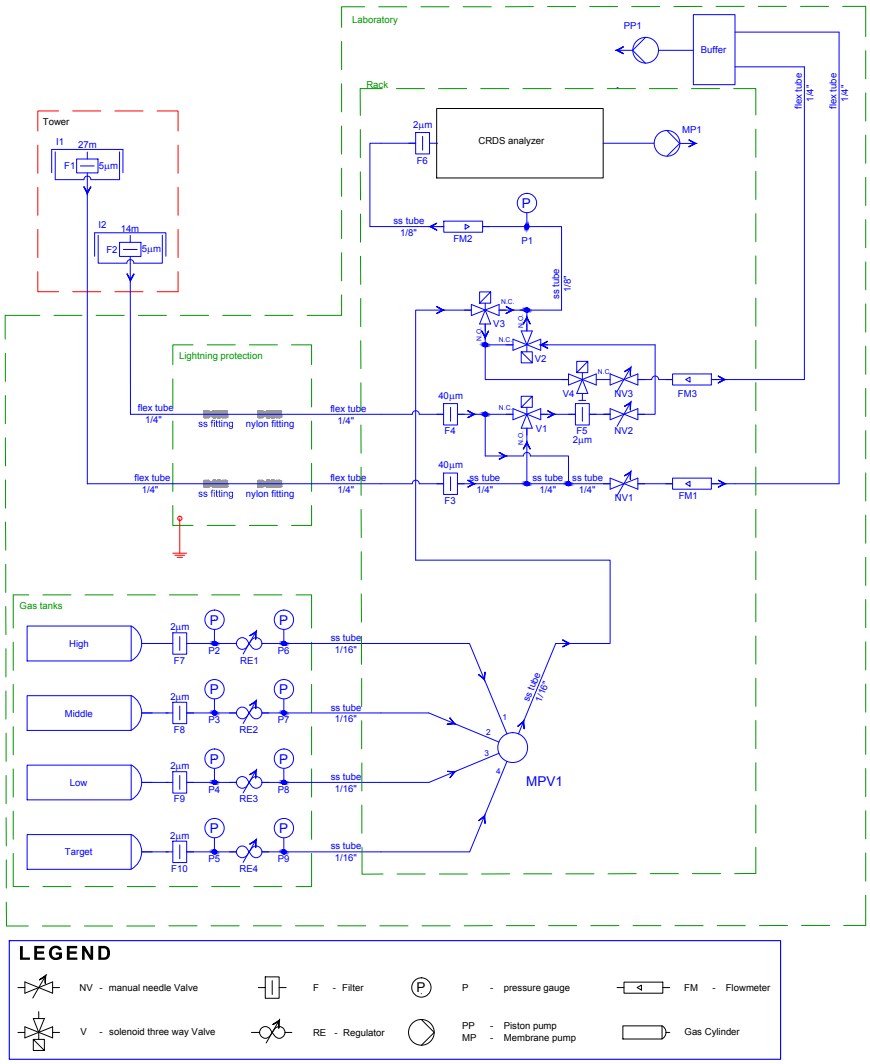

Fig. 3: Air flow diagram of Ambarchik greenhouse gas measurement system. See Sect. 2.3 for a description of component abbreviations.

2.4 Meteorological measurements

Meteorological measurements performed by MPI-BGC at Ambarchik include wind speed and direction at 20 m a.g.l., air temperature and humidity at 20 and 2 m a.g.l., and air pressure at 1 m a.g.l. (instruments listed in Table A.2). The measurements mainly serve to monitor atmospheric conditions like wind and stability of atmospheric stratification for quality control of the GHG data (described in Sect. 3.4). The 2D sonic anemometer, which is used to measure wind speed and direction, features a built-in heating to prevent freezing. The heating is switched on if temperature decreases below 4.5 °C and relative humidity is higher than 85 %, and switched off when temperatures increase above 5.5 °C.

2.5 Power supply

Power is supplied by the diesel generator of the Roshydromet meteorological station. Power consumption of the MPI-BGC measurement system is about 350 W, and an additional 125 W is required in case the heating of the sonic anemometer is switched on. In order to avoid loss of power during routine generator maintenance, an uninterruptible power supply (9130 UPS, Eaton) was installed, which is able to buffer power outages of up to about 40 minutes (the heating of the sonic anemometer is not powered by the UPS). In case of a longer power loss, the UPS initiates a controlled shutdown of the CRDS analyzer.

2.6 Data logging

Trace gas measurements and related data are logged by the factory-installed software of the CRDS analyzer. All other measurements are logged by an external data logger (CR3000, Campbell Scientific). The logger samples all variables every 10 seconds. Raw samples are stored for wind measurements as well as flow and pressure in the tubing (FM1–FM3, P1). Of the remaining meteorological measurements, room and rack temperature, and diagnostic variables, 10-minute averages are stored. The data are transferred from the external data logger to the hard drive of the CRDS analyzer daily. All data is backed up to an external hard drive hourly. The internal clocks of the CRDS analyzer and the data logger are synchronized with a GPS receiver (GPS 16X-HVS, Garmin) once per day.

3 Quality control

3.1 Water correction

In order to minimize maintenance efforts and reduce the number of components prone to failure, CO_2 and CH_4 mole fractions are measured in humid air. Hence, the values reported by the analyzer have to be corrected for the effects of water vapor to obtain dry air mole fractions. This is done by applying a water correction function to the raw data:

$$\boldsymbol{c_{dry}} = \frac{\boldsymbol{c_{wet}}(\boldsymbol{h})}{f_c(\boldsymbol{h})} \quad (1)$$

Here, $\boldsymbol{c_{wet}}$ is the mole fraction of CO_2 or CH_4 in humid air reported by the analyzer, h is the water vapor mole fraction (also measured by the CRDS analyzer), $f_c(\boldsymbol{h})$ is the water correction function, and $\boldsymbol{c_{dry}}$ is the desired dry air mole fraction. Picarro Inc. provides a factory water correction based on Chen et al. (2010), but to achieve accuracies within the WMO goals for water vapor mole fractions above 1 % H_2O, custom coefficients must be obtained for each analyzer (Rella et al., 2013). Here, we employ the novel water correction method by Reum et al. (2019). In Reum et al. (2019), data from gas washing bottle experiments (explained in Appendix B) with the CRDS analyzer in Ambarchik were analyzed in the context of the new method (labeled "Picarro #5" therein). Here, we use these data together with data from additional experiments to derive water correction coefficients for the application to the complete Ambarchik record. The results of this procedure are briefly summarized here, while more details are given in Appendix B.

Water correction experiments have been performed in 2014, 2015 and 2017. Differences between the water corrections based on the different experiments were on the order of magnitude of the WMO goals (Fig. 4). Here, we chose the WMO internal reproducibility goals as reference, which correspond to half of the interlaboratory compatibility goals (WMO, 2016). The motivation for this choice is that keeping biases of observations with respect to the calibration scale within these goals ensures that biases between stations are within the interlaboratory compatibility goals. Given the small number of water correction experiments conducted so far, it is unknown whether these differences represent drifts over long time scales, short-term variations and/or systematic differences between the experimental methods. Stavert et al. (2019) found that variability among weekly water correction tests over three months was

Revision 2.9.2019 11:07
Gelöscht: (2018). Results

Revision 2.9.2019 11:07
Gelöscht: Given the small number of experiments conducted so far, it is unknown whether these differences represent drifts over long time scales, short-term variations and/or systematic differences between the experimental methods. Therefore, water correction coefficients were derived based on the averages of the individual water correction function responses for each species. The maximum deviations of the individual functions to the

similar as that of annual tests over two years. This indicates that the differences of the Ambarchik analyzer could be short-term variations. In the absence of evidence for trends, water correction coefficients were derived based on the averages of the individual water correction function responses for each species (see Appendix B). The maximum deviations of the individual functions to these synthesis functions were 0.018 % CO_2 at 3 % H_2O, which corresponds to 0.07 ppm at 400 ppm dry air mole fraction, and 0.034 % CH_4 at 2.7 % H_2O, which corresponds to 0.7 ppb at 2000 ppb dry air mole fraction (Fig. 4).

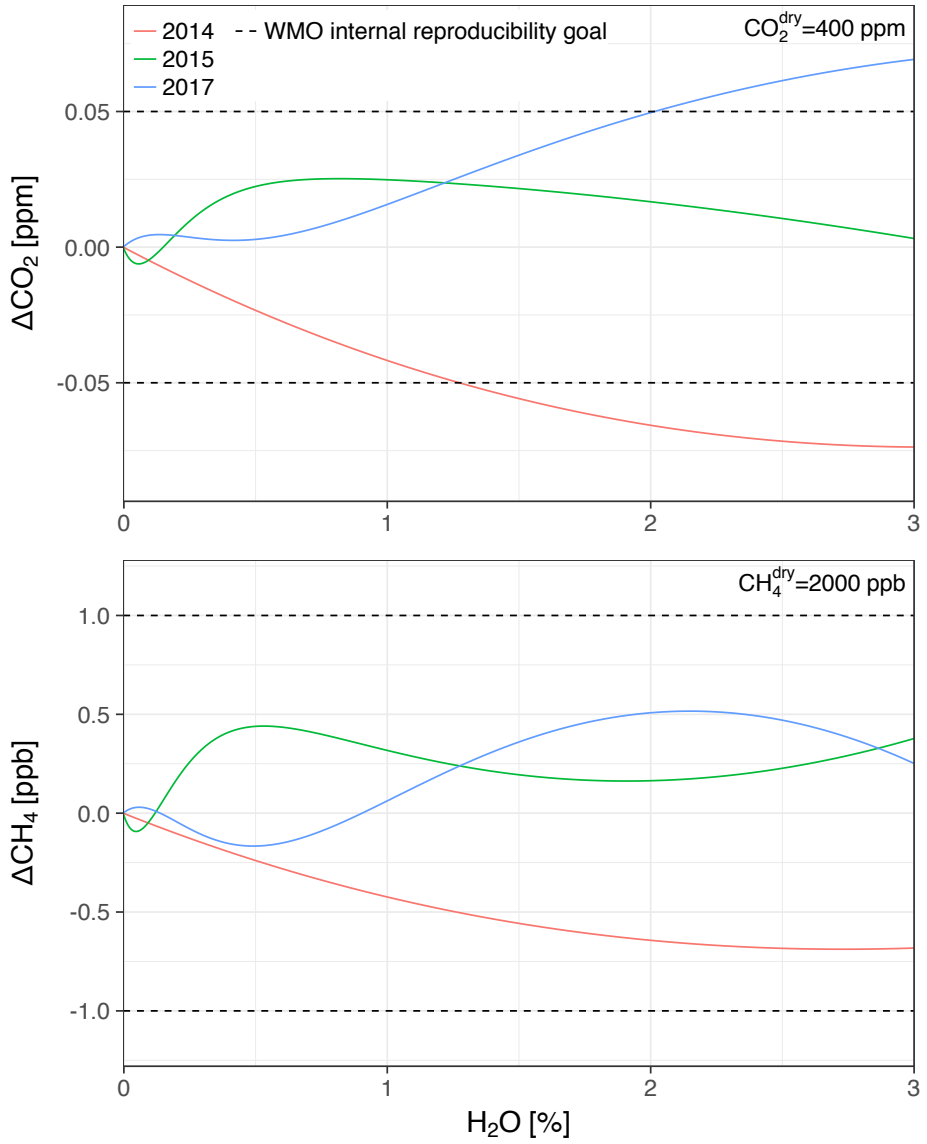

Revision 2.9.2019 11:07

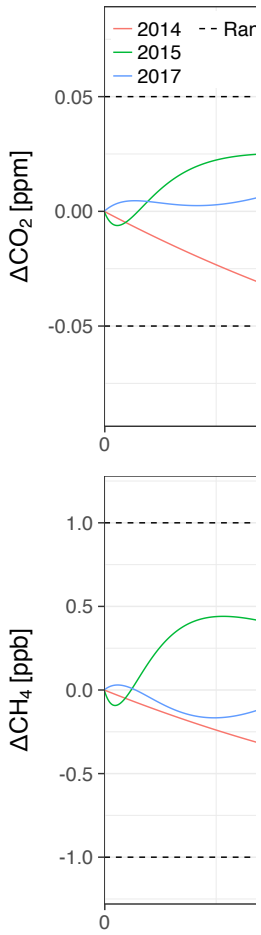

Gelöscht:

Fig. 4: Differences between individual water correction functions and the synthesis water correction function at dry air mole fractions of 400 ppm CO_2 and 2000 ppb CH_4. The dashed lines correspond to the WMO internal reproducibility goals in the case of CO_2 in the northern hemisphere (WMO, 2016).

Revision 2.9.2019 11:07
Gelöscht: (

Revision 2.9.2019 11:07
Gelöscht:), a value that incorporates uncertainties in transferring the calibration scale from the highest level of standards to working standards and other uncertainties, for example related to gas handling

3.2 Calibration

Calibrations are performed with a set of pressurized dry air tanks filled at the Max Planck Institute for Biogeochemistry (Jena, Germany). The levels of GHG mole fractions of these tanks have been traced to the WMO scales X2007 for CO_2 and X2004A for CH_4 (Table C.1). Three calibration tanks (in order High, Middle, Low) are probed once every 116 hours for 15, 10 and 10 minutes, respectively. The longer probing time of the first (High) tank serves to flush out residual water vapor due to water molecules that adhere to the inner tubing walls. Thus, residual water vapor during tank measurements is well below 0.01 % H_2O. From these three tanks, coefficients for linear calibration functions are derived. Due to the scatter of the coefficients over time, the coefficients are smoothed using a tricubic kernel with a width of 120 days (Fig. C.1). Individual measurements are calibrated by applying the smoothed coefficients, interpolated linearly in time. The impact of the smoothing on the calibration of ambient mole fractions is smaller than 0.02 ppm CO_2 and 0.3 ppb CH_4 (one standard deviation). The fourth tank (Target) is probed every 29 hours for 15 minutes. Its calibrated CO_2 and CH_4 mole fraction measurements (Fig. 5) serve as quality control of the calibration procedure (Sect. 3.3). Uncertainties associated with the calibration procedure, as well as possible future improvements, are discussed and quantified in Appendix E.

Revision 2.9.2019 11:07
Gelöscht: out of

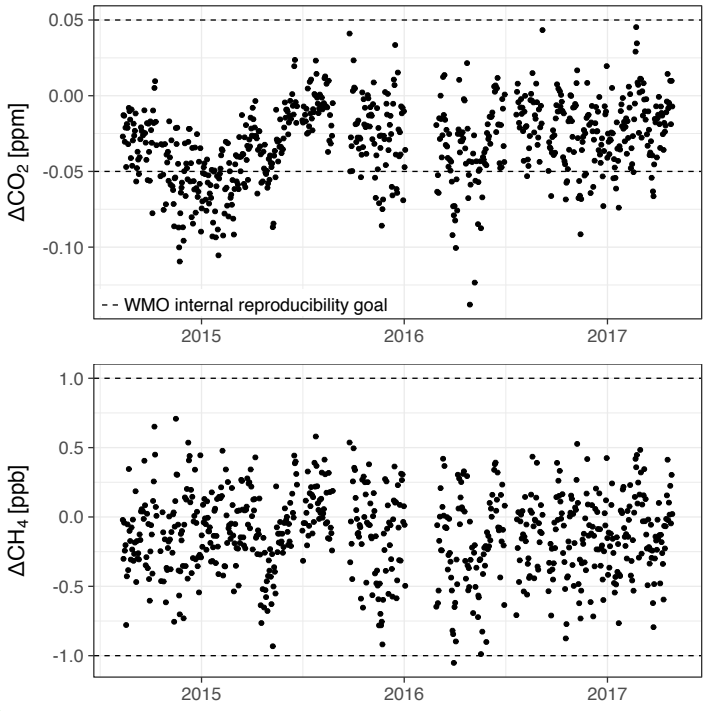

Fig. 5: Target tank bias over time for CO_2 and CH_4. As in Fig. 4, the dashed lines correspond to the WMO internal reproducibility goals.

3.3 Uncertainty in CO_2 and CH_4 measurements

Measurement uncertainties in the CO_2 and CH_4 data arise from instrument precision, the calibration and the water correction. We estimated time-varying uncertainties of hourly trace gas mole fraction averages based on the method by Andrews et al. (2014), with some modifications. Details of the procedure are in Appendix E.

Average uncertainties at 1σ-level were 0.085 ppm CO_2 and 0.77 ppb CH_4. Both were dominated by the variability between the water vapor correction experiments. The contribution of analyzer signal

Revision 2.9.2019 11:07
Gelöscht:
Revision 2.9.2019 11:07
Gelöscht: cover
Revision 2.9.2019 11:07
Gelöscht: 11
Revision 2.9.2019 11:07
Gelöscht: 75

precision for averages over one hour to these uncertainties was 0.013 ppm CO_2 and 0.25 ppb CH_4. These numbers may be used to distinguish analyzer signal precision from atmospheric variability.

3.4 Data screening

After water correction and calibration, invalid data are automatically removed before calculating hourly averages using filters for bad analyzer status (Sect. 3.4.1), flushing of lines (Sect. 3.4.2), times of calibration and maintenance, contamination from local polluters (Sect. 3.4.3) and water vapor spikes (Sect. 3.4.4). In the case of contamination from local polluters, CO_2 and CH_4 averages are also computed with the flagged data to allow assessing the impact of the filter. Additional variables reported in the hourly averages allow for further data screening, e.g. for using the data in inverse models (Table 1). Details on the gradient of virtual potential temperature are given in Sect. 3.4.5.

Table 1: Variables for data screening and an example for a strict filter for background conditions that was used to infer average growth rates in Sect. 5.1.

Variable	Background filter example
Mole fractions without removing CO_2 spikes	Remove flagged spikes
Difference between inlets	$\lvert\Delta CO_2\rvert < 0.1$ ppm; $\lvert\Delta CH_4\rvert < 2$ ppb
Intra-hour variability	$\sigma(CO_2) < 0.2$ ppm; $\sigma(CH_4) < 4$ ppb
Gradient of virtual potential temperature	$\Delta T_{v,p} < 0$ K
Wind speed	$w_v > 2$ ms^{-1}
Time of day	1 pm – 4 pm

Revision 2.9.2019 11:07
Gelöscht: trends (

Revision 2.9.2019 11:07
Gelöscht:).

3.4.1 Analyzer status diagnostics

Picarro Inc. provides the diagnostic flags INST_STATUS and ALARM_STATUS that monitor the operation status of the analyzer. The values in Table 2 indicate normal operation. The flag ALARM_STATUS indicates both exceeding user-defined thresholds for high mole fractions (ignored here), and data flagged as bad by the data acquisition software. The code reported in INST_STATUS contains, among other indicators, thresholds for cavity temperature and pressure deviations from their

target values. We created stricter filters for these two values based on their typical variation during normal operation of this particular measurement system. Occasionally, small numbers (< 5) of outliers are recorded after a period of lost data (e.g. due to high CPU load). These are removed manually.

Table 2: Diagnostic values indicating normal status of the CRDS analyzer.

Quantity	Filter
INST_STATUS	INST_STATUS = 963
ALARM_STATUS	ALARM_STATUS < 65536
Cavity temperature	$\lvert T_c - 45°\ C\rvert < 0.0035$ K
Cavity pressure	$\lvert p_c - 186.65$ hPa$\rvert < 0.101$ Pa

3.4.2 Flushing of measurement lines

Air from the two inlets at the tower and the calibration tanks flows through some common tubing (Fig. 3). Hence, air measured immediately after a switch is influenced by the previous air source. We remove the first 30 seconds from the record after a switch between inlets to avoid sample cross-contamination. Air from calibration tanks exhibits larger differences in humidity and mole fractions to ambient air. Hence, the first five minutes of ambient air measurements after tank measurements are removed from the record.

3.4.3 Contamination from local polluters

Possible frequent contamination sources in the immediate vicinity of the tower are the building hosting the power generator of the facility (65 m northwest from tower), the heating and oven chimneys of the only inhabited building (30 m and 20 m northeast, respectively) and waste disposal. These local polluters can cause sharp and short increases in CO_2 and CH_4 mole fractions on the timescale of seconds to a few minutes. These features cannot be modeled by a regional or global atmospheric transport model and should therefore be filtered out. We developed a detection algorithm to identify spikes based on their duration, gradients, and amplitude in the raw CO_2 data. Spike detection algorithms are often compared to manual flagging by station operators (El Yazidi et al., 2018). Parameters of our algorithm

Revision 2.9.2019 11:07

Gelöscht:) and the heating and oven chimneys of the only inhabited building (30 m and 20 m northeast, respectively). These local polluters can cause sharp and short increases in CO_2 (and, depending on the source, CH_4) mole fractions on the timescale of seconds to a few minutes. These features cannot be modeled by a regional or global atmospheric transport model and should therefore be filtered out. We developed a detection algorithm to identify spikes based on their duration, gradients, and amplitude in the raw CO_2 data. Spike detection algorithms are often compared to manual flagging by station operators (El Yazidi et al., 2018). Parameters of our algorithm were tuned in this way based on the first year of data. Large CH_4 spikes often coincided with CO_2 spikes. Hence, the spike detection algorithm was developed for CO_2 and used to flag both CO_2 and CH_4, although this may remove some unpolluted CH_4 signals.

were tuned in this way based on the first year of data. The algorithm is described in Appendix D. The impact of the CO_2 spike flagging procedure is shown in Table 3. Impacts on the hourly mole fractions are small, more so when considering only data that pass other quality filters.

We observed that large CH_4 spikes were much less frequent than and often coincided with CO_2 spikes. Hence, the spike detection algorithm developed for CO_2 was used to flag CH_4 as well. This strategy may remove some unpolluted CH_4 signals and, in rare cases, leave contaminated CH_4 signals undetected. However, given the small impact of filtering flagged CO_2 spikes and the smaller frequency of large CH_4 spikes, we think that contamination of CH_4 independent of CO_2 is a negligible source of error in Ambarchik data. Furthermore, due to the large variability of natural CH_4 sources, a spike detection algorithm for CH_4 may bear the risk of flagging natural signals. In addition, CH_4 contamination may also be flagged based on other criteria, in particular their intra-hour variability. For these reasons, we decided that a common filter for both CO_2 and CH_4 works best at Ambarchik.

Table 3: Fraction of hourly averages of all data from the Top inlet that contain flagged CO_2 spikes, and impact of removing them before averaging (ΔCO_2, ΔCH_4).

Metric	All data	Data with $w_v > 2$ ms^{-1} and $\Delta T_{v,p} < 0$ K
Cases that contain flagged spikes	15 %	6 %
Cases where $\Delta CO_2 > 0.1$ ppm	4 %	< 1 %
Cases where $\Delta CH_4 > 2$ ppb	< 1 %	< 1 %
Mean / median ΔCO_2	0.16 / 0.03 ppm	0.07 / 0.02 ppm
Mean / median ΔCH_4	0.5 / 0.03 ppb	0.2 / 0.02 ppb

3.4.4 Water vapor spikes

During winter, the CRDS analyzer occasionally records H_2O spikes with durations of a few seconds. The spikes typically exhibit much higher mole fractions than possible given ambient air temperature. This suggests that they are caused by small amounts of liquid water in the sampling lines in the laboratory upon evaporation. Since we observed the phenomenon exclusively during the cold season, we speculate that it is caused by small ice crystals that may form on the air inlet filters (F1, F2), detach, are trapped by one of the filters inside the laboratory, and evaporate.

Since fast water vapor variations deteriorate the accuracy of the water vapor correction, we remove the spikes before creating hourly averages. Spikes are identified using a flagging procedure similar to the one for CO_2 contamination described in Appendix D, with parameters adapted to the different shape of the H_2O spikes.

3.4.5 Virtual potential temperature

Regional and global scale atmospheric tracer transport models rely on the assumption that the boundary layer is well-mixed (e.g. Lin et al., 2003). This requirement is not satisfied when the air is stably stratified due to a lack of turbulent mixing (Stull, 1988). This may occur when the virtual potential temperature increases with height. To detect these situations, sensors for temperature and relative humidity are installed at 2 m and 20 m above ground level on the measurement tower (Table A.2). Based on these measurements, the virtual potential temperature is calculated for both heights, and the difference can be used as an indicator for stable stratification of the atmospheric boundary layer at the station (e.g. Table 1 and Sect. 5.1).

4 Atmospheric tracer transport to Ambarchik

The predominant wind directions at Ambarchik were southwest and northeast (Fig. 6) over the analyzed period (8/2014 – 4/2017). Southwesterly winds dominated from October to March, while northeasterly winds dominated from April to August. September and October were a transitional period.

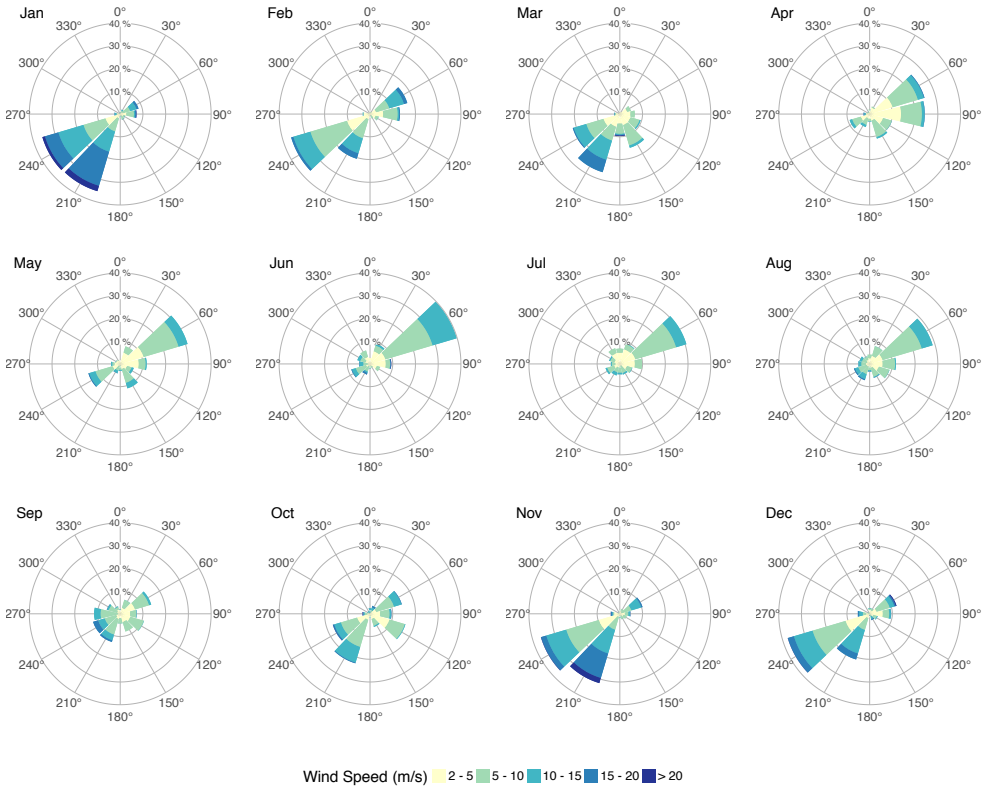

Fig. 6: Wind distribution at Ambarchik for wind speeds > 2 ms^{-1} for the period 8/2014 – 4/2017.

We used an atmospheric transport model (Henderson et al., 2015) to determine regions within the Arctic that influence the atmospheric signals captured at Ambarchik. For the case studies shown here, 15-day backtrajectories were calculated for the period August 2014 to December 2015. Atmospheric transport was modeled using STILT (Lin et al., 2003) driven by WRF (Skamarock et al., 2008), for which boundary and initial conditions were taken from MERRA reanalysis fields (Rienecker et al., 2011). The resolution of the transport model in our domain was mostly 10 km horizontally with 41 vertical levels. Based on these trajectories, the sensor source weight functions ("footprints") were calculated on a

square-shaped lambert azimuthal equal area grid with a resolution of 32 km and an extent of 3200 km centered on Ambarchik. To better visualize the representativeness of Ambarchik data to different origins of air masses, we aggregated these footprints over seasons. Furthermore, we sorted the aggregated footprints into bins each covering a quartile of the cumulative footprint (Fig. 7). Footprints covered adjacent northeast Siberian tundra and taiga ecoregions as well as the East Siberian Arctic Shelf, with seasonally varying influences. In winter, spring and summer, the top quartile of the footprint concentrated on a few grid cells (order of ~100 km) around Ambarchik, with a slightly larger spread in fall. The two central quartiles had a focus on easterly directions in spring and on the north in summer.

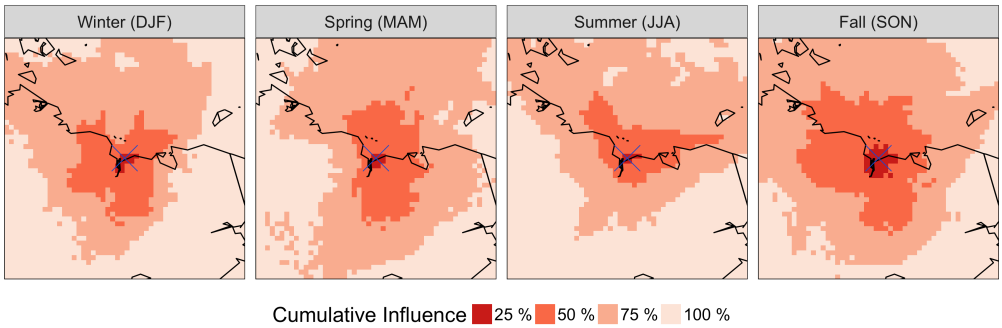

Fig. 7: Cumulative Ambarchik footprints based on 15-day backtrajectories for 08/2014–12/2015. The footprints were aggregated over the seasons winter (December-January-February), spring (March-April-May), summer (June-July-August) and fall (September-October-November), and sorted into bins covering 25 % of the cumulative influence each. Shown here is a two-fold zoom on the center of the domain, covering 1600 km × 1600 km.

5 Greenhouse gas signals at Ambarchik

5.1 Ambarchik time series in comparison with Barrow, Alaska

In order to provide a context for the characteristics of greenhouse gas signals measured at Ambarchik, we compared the time series from Ambarchik with in-situ CO_2 (NOAA, 2015) and CH_4 (Dlugokencky et al., 2017) mole fractions observed at Barrow, Alaska Observatory, which is located close to the village of Utqiaġvik (71.32° N, 156.61° W). Data from Barrow were chosen for the comparison because of the station's proximity to Ambarchik (distance ~1.500 km, latitudinal difference 1.7°; cf. Fig. 1), and because they have been used in many studies on both global and regional greenhouse gas fluxes (e.g.

Berchet et al., 2016; Jeong et al., 2018; Rödenbeck, 2005; Sweeney et al., 2016). The analyzed period was August 2014 to December 2016.

For the comparison, afternoon data (1–4 pm) for which the wind speed was above 2 ms^{-1} were used (gaps in the MPI-BGC wind measurements were filled with Roshydromet 10 m wind speed data). In addition, Ambarchik data were filtered out when the virtual potential temperature increased with height. This filter was omitted for Barrow, because it would have removed most of the data from October to April, including data classified as "background" signals (which occurred throughout the year). Barrow data were filtered according to their quality flag. For CO_2, data with quality flags "...", ".D.", ".V." and ".S." were included. For CH_4, data with quality flags "..." and ".C." were included. Data with other flags than a "." in the first column were removed as invalid. Other quality flags (differing in the second or third column) were excluded because their number was negligible. We inferred average growth rates and seasonal cycles for the analyzed period based on the curve fitting procedure by Thoning et al. (1989): linear trends and four harmonics representing the seasonal cycles were fitted to the data, and a low-pass filter was applied to the residuals. We emphasize that the purpose of this procedure was not to infer baselines, which would not be suitable for CH_4. Instead, the fitted curves were smooth representations of the time series, including regional signals. To minimize the influence of interannual variations on the estimated average growth rates at Ambarchik, they were estimated with additional strict filters for background conditions applied to Ambarchik data (Table 1). Given the short duration of the Ambarchik record, we estimated seasonal cycle amplitude and timing based on the harmonic part of the fit function, which was more robust than including smoothed residuals.

Revision 2.9.2019 11:07
Gelöscht: To infer trends and seasonal cycles, we applied the curve fitting procedure by Thoning et al.

Revision 2.9.2019 11:07
Gelöscht: The

Revision 2.9.2019 11:07
Gelöscht: trends

Revision 2.9.2019 11:07
Gelöscht: data

Revision 2.9.2019 11:07
Gelöscht: particularly sensitive to interannual variations. Therefore,

Revision 2.9.2019 11:07
Gelöscht: were

Revision 2.9.2019 11:07
Gelöscht:) to obtain trends.

5.1.1 Carbon dioxide

In spring, CO_2 mole fractions observed at Ambarchik closely tracked those measured at Barrow (Fig. 8), which was likely due to the absence of local to regional sources and sinks during this period. In summer, Ambarchik recorded a stronger seasonal drawdown of CO_2 mole fractions compared to Barrow, leading to a lower minimum value that occurred 12 days earlier. In fall, CO_2 rose faster at Ambarchik, reaching the midpoint between minimum and maximum 21 days earlier compared to Barrow. The mole fraction maxima in winter were at similar values. Carbon dioxide mole fractions at

Ambarchik were more variable than at Barrow in summer and fall, which indicates stronger local and regional sources and sinks captured by the Ambarchik tower. The annual amplitude of CO_2 was slightly larger at Ambarchik (20 ppm vs. 18 ppm) because of the lower summer minimum. The average growth rates were (2.77 ± 0.09) and (2.82 ± 0.05) ppm CO_2 yr^{-1} at Ambarchik and Barrow, respectively. Note that despite the good agreement of these growth rates, their uncertainties are larger than the statistical uncertainties given here, since the estimates depended on data selection and were based on less than three years of data. We note that in November and December 2016, exceptionally high CO_2 mole fractions were measured at Ambarchik. However, analysis of individual signals is beyond the scope of this paper.

Revision 2.9.2019 11:07
Gelöscht: trends

Revision 2.9.2019 11:07
Gelöscht: the trends

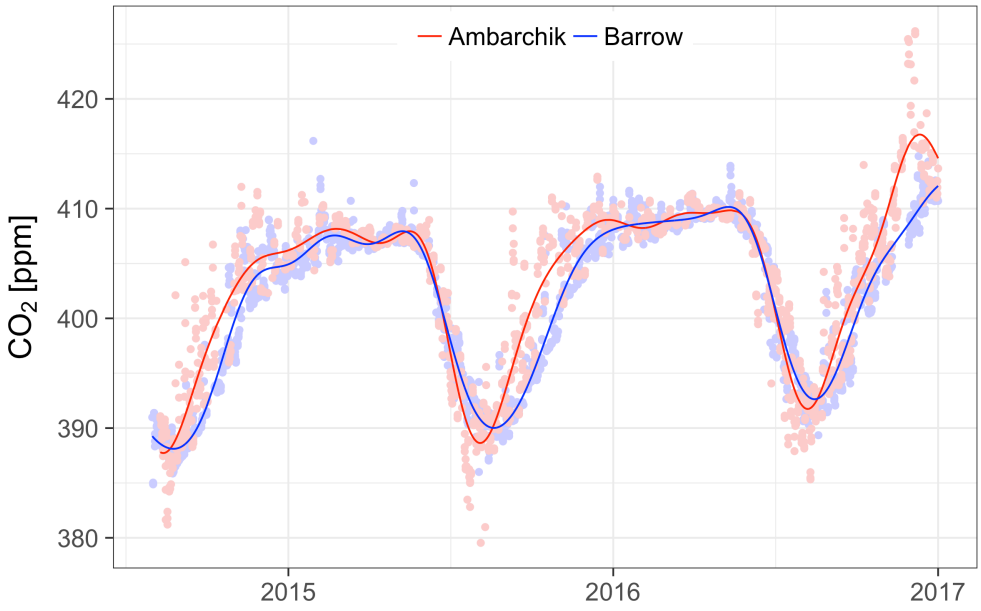

Fig. 8: Atmospheric CO_2 and CH_4 measurements from Ambarchik and Barrow. Points are quality-controlled hourly averages; lines are the results of a curve fit plus smoothed residuals (see text for details).

5.1.2 Methane

Similar to CO_2 mole fractions, in spring, CH_4 mole fractions at Ambarchik matched those at Barrow and had low variability (Fig. 8). Throughout the rest of the year, CH_4 mole fractions at Ambarchik were higher and more variable than at Barrow, which is reflected by the larger annual amplitude of 72 ppb at Ambarchik, compared to 47 ppb at Barrow. The summer minimum of the harmonics occurred 70 days earlier at Ambarchik. By contrast, the minimum of the visual baseline of hourly data occurred much later, and was close in values and timing compared to the Barrow measurements (Fig. 9). This discrepancy was due to the fact that the harmonics fitted to Ambarchik CH_4 data were influenced by large positive CH_4 enhancements starting in early summer, which are likely caused by strong regional sources. Such CH_4 enhancement events were also recorded throughout most of the winters. Estimated average growth rates of CH_4 were (6.4 ± 1.0) ppb yr^{-1} at Ambarchik and (10.0 ± 0.7) ppb yr^{-1} at Barrow. Note that, as for CO_2, the true uncertainties of these growth rates are larger than the statistical uncertainties given here, since the estimates depended on the data selection.

Revision 2.9.2019 11:07
Gelöscht: trends

Revision 2.9.2019 11:07
Gelöscht: the trends

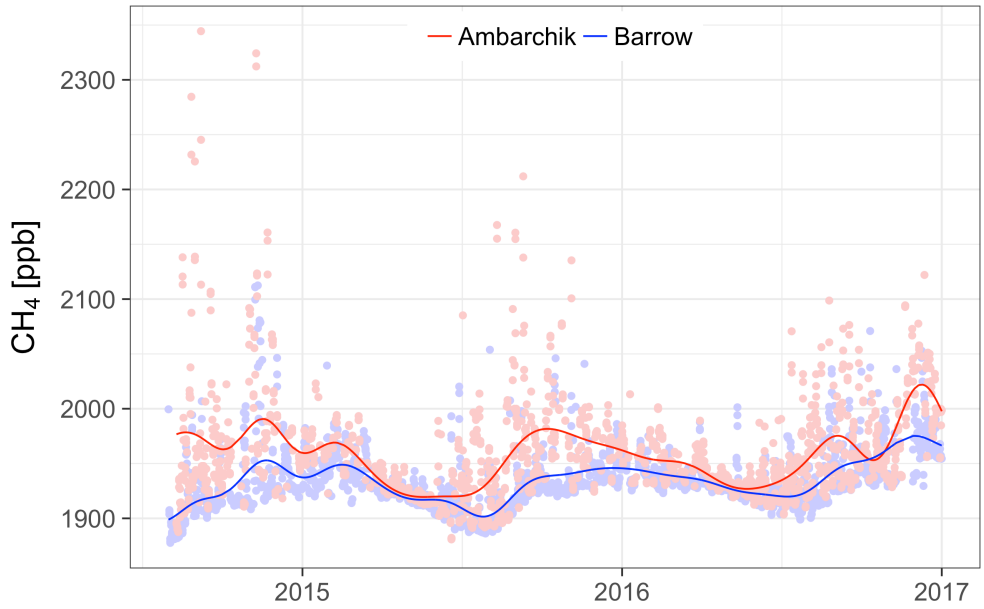

Fig. 9: Same as Fig. 8, but for CH_4.

5.2 Angular distribution of regional CO_2 and CH_4 anomalies

Ambarchik is located at a junction of several different ecoregions, and in particular at the coast of the East Siberian Sea. Therefore, the dependence of CO_2 and CH_4 signals on wind direction could provide insights into CO_2 and CH_4 exchange between these different regions and the atmosphere. We examined this dependence based on CO_2 and CH_4 anomalies representative of fluxes inside the domain introduced in Sect. 4 (3200 km × 3200 km, centered on Ambarchik). These anomalies were computed following a standard method in regional inverse modeling of atmospheric tracer transport, i.e. by subtracting the contribution of CO_2 and CH_4 transported into the domain (the background signal) from the observations. The anomalies therefore represent the atmospheric signature of sources and sinks inside the domain. The background signal was computed by sampling global atmospheric CO_2 and CH_4 mole fraction fields at the end points of the backtrajectories introduced in Sect. 4. The global CO_2 fields were

Revision 2.9.2019 11:07
Gelöscht: We examined whether CO_2 and CH_4 signals measured at Ambarchik were distinguishable by wind direction. For this purpose, anomalies were computed as differences between the measurements at Ambarchik and a baseline, which

Revision 2.9.2019 11:07
Gelöscht: These anomalies therefore represent the atmospheric signature of regional sources and sinks captured at Ambarchik.

based on Rödenbeck (2005, version doi:10.17871/CarboScope-s04_v3.8.), and the CH_4 fields were based on the code by Rödenbeck (2005) modified by T. Nunez-Ramirez (personal communication). Both fields were optimized for station sets that included Ambarchik data. We analyzed the data that passed the filters for low wind speeds and temperature inversions (see Table 1) grouped by season, and focused the interpretation on the signals from the predominant wind directions, since sample sizes from other sectors were small.

5.2.1 Carbon dioxide

The most pronounced CO_2 signals from predominant wind directions were positive anomalies during southwesterly winds in fall and winter. During summer, CO_2 anomalies from the predominant wind direction (northeast) were small. During spring, almost no CO_2 anomalies were observed.

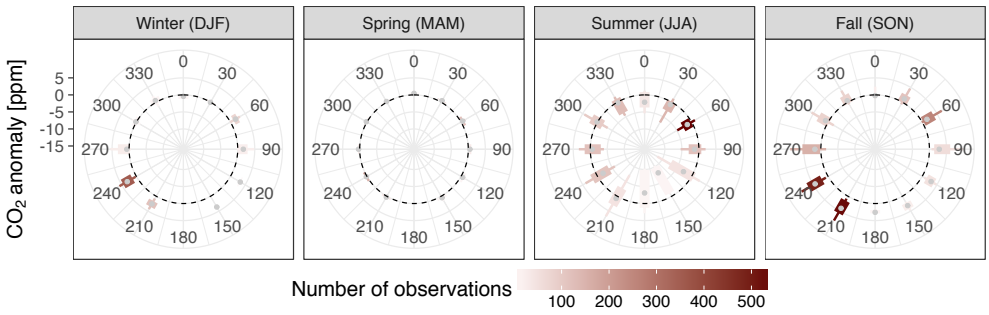

Fig. 10: Carbon dioxide anomalies plotted against wind direction. The dashed circle is the baseline (anomaly 0 ppm). The (grey) points are the median, boxes the first and third quartile, and whiskers the first and ninth decile. Shown here are data that passed the filters for low wind speeds and temperature inversions (Table 1). The color of boxes and whiskers indicates the number of measurements available in each bin.

5.2.2 Methane

The strongest CH_4 enhancements were observed from westerly winds in summer, and southwesterly winds in fall and winter. The predominant northeasterly winds in summer carried comparatively small CH_4 enhancements. The overall variability of CH_4 was highest in summer and fall, with considerable enhancements especially from the southwest in winter. Like CO_2, CH_4 showed almost no anomalies in spring.

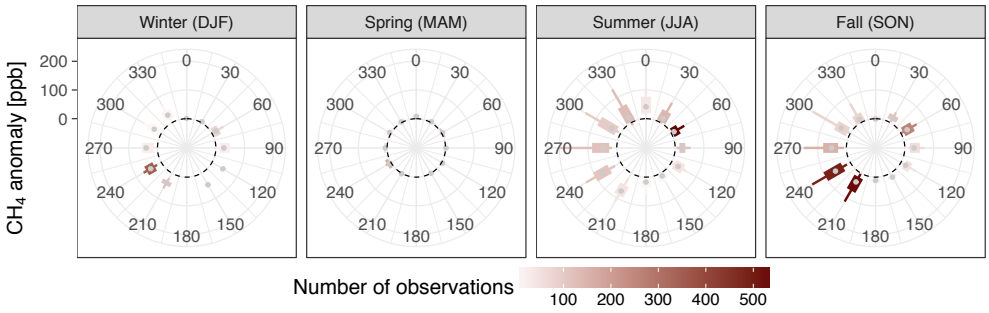

Fig. 11: Same as Fig. 10, but for CH_4

6 Discussion and conclusions

In this paper, we presented the first years (August 2014 – April 2017) of CO_2 and CH_4 measurements from the coastal site Ambarchik in northeast Siberia. The site has been operational without major downtime since its installation. Greenhouse gas measurements are calibrated about every five days using dry air from gas tanks with GHG mole fractions traced to WMO scales. Mole fractions of CO_2 and CH_4 are measured in humid air and corrected for the effects of water vapor using a novel water vapor correction method. An algorithm was developed to remove measurements influenced by local polluters, which affected a small fraction of the measurements. Measurements of the gradient of the virtual potential temperature and the two sampling heights allow for detection of stable stratifications of the atmospheric boundary layer at the station. Uncertainties of the GHG measurements, which were inferred from measurements of dry air from calibrated gas tanks and water correction experiments, were on average 0.085 ppm CO_2 and 0.77 ppb CH_4. We continue work on improvements of the accuracy of the calibrations and uncertainty estimates and will adapt them as additional information becomes available (e.g. based on post-deployment calibration of used gas tanks).

A footprint analysis indicates that Ambarchik is sensitive to trace gas emissions from both the East Siberian Sea and terrestrial ecosystems. Both CO_2 and CH_4 anomalies were large during southwesterly and westerly winds and small during northeasterly winds. This suggests that the larger signals originated from terrestrial rather than oceanic fluxes and demonstrates the value of sampling at the

Revision 2.9.2019 11:07
Gelöscht: estimated based on

Revision 2.9.2019 11:07
Gelöscht: 11

Revision 2.9.2019 11:07
Gelöscht: 75

Revision 2.9.2019 11:07
Gelöscht: , with potential

Revision 2.9.2019 11:07
Gelöscht: by future experiments. Thus,

Revision 2.9.2019 11:07
Gelöscht: CO_2 uncertainties exceeded

Revision 2.9.2019 11:07
Gelöscht: WMO inter-laboratory compatibility goal in the northern hemisphere (0.1 ppm CO_2), while the CH_4

Revision 2.9.2019 11:07
Gelöscht: was well within the WMO goal of 2 ppb CH_4.

Revision 2.9.2019 11:07
Gelöscht: , which

location of Ambarchik for distinguishing fluxes from different source regions and thus insights into carbon cycle processes in this region. In comparison with Barrow, Alaska, Ambarchik recorded larger CO_2 and CH_4 anomalies, which resulted in larger seasonal cycle amplitudes as well as earlier minima and fall growth. We interpret the stronger CO_2 and CH_4 signals at Ambarchik as stronger local and regional fluxes compared to those captured at Barrow. Strong CH_4 enhancements were recorded at Ambarchik well into the winter, which is evidence for the relevance of cold season emissions (Kittler et al., 2017b; Mastepanov et al., 2008; Zona et al., 2016). While the average growth rate of CO_2 at Ambarchik matched the one at Barrow, the growth rate of CH_4 at Ambarchik was smaller. We attribute the discrepancy to the short analysis period, which makes the growth rate estimate sensitive to interannual variability and differences in the timing of the annual maximum and minimum.

The accuracy of the CO_2 and CH_4 data obtained at Ambarchik, and their sensitivity to sources and sinks of high-latitude terrestrial and oceanic ecosystems make the Ambarchik station a highly valuable tool for carbon cycle studies focusing on both terrestrial and oceanic fluxes from Northeast Siberia.

Revision 2.9.2019 11:07
Gelöscht: trend

Revision 2.9.2019 11:07
Gelöscht: trend

Revision 2.9.2019 11:07
Gelöscht: trend

Appendix A Hardware manufacturers and models

Table A.1: Gas handling components

Description	Label	Manufacturer	Model
CRDS analyzer	CRDS analyzer	Picarro	G2301
Membrane pump	MP1	Picarro	Picarro vacuum pump
Piston pump	PP1	Gardner Denver Thomas	617CD32
Flow meter	FM1	OMEGA	FMA1826A
Flow meter	FM2	OMEGA	FMA1814A-ST
Flow meter	FM3	OMEGA	FMA1812A
Multiposition valve	MPV1	Vici	Valco EMT2CSD6MWM
Solenoid valve	V1–V4	SMC	VDW350-6W-2-01N-H-X22-Q
Needle Valve	NV1–NV3	Swagelok	SS-2MG

Gas tanks	High, Middle, Low, Target	Luxfer Gas Cylinders	20 l T-PED cylinders, Type P3056Z
Pressure regulator	RE1–4 (incl. pressure gauges P2–P9)	TESCOM	44-3440KA412-S
Pressure sensor	P1	Keller	PAA-21Y
Stainless steel tubing	ss tube 1/16”	Vici	Vici Jour JR-T-625-40
Stainless steel tubing	ss tube 1/8”	Vici	Vici Jour JR-T-626-00
Flexible tubing	flex tube 1/4”	SERTO	SERTOflex 6.35S
Inlet filter	F1, F2	Solberg	F-15-100
Filter	F3, F4	Swagelok	SS-4TF-40
Filter	F5, F6	Swagelok	SS-4FW-2

Table A.2: Meteorological measurements by MPI-BGC at Ambarchik

Measurand	Manufacturer	Model	Height a.g.l. / location
Wind speed, direction	METEK	uSonic-2	20 m / tower
Air temperature, relative humidity	MELA	KPK1_6-ME-H38 (inside ventilated radiation shield)	20 m and 2 m / tower
Air pressure	SETRA	Type 278	1 m / laboratory

Appendix B Derivation of water correction coefficients

The influence of water vapor on CO_2 and CH_4 measurements was corrected for based on several water correction experiments and a novel water correction model, which we describe in the following paragraphs. For more details, please refer to Reum et al. (2019). As stated in Sect. 3.1, data from gas washing bottle experiments (explanation below) with the CRDS analyzer located in Ambarchik were analyzed in Reum et al. (2019) in the context of the new water correction method (labeled “Picarro #5” therein). Here, we use these data together with data from additional experiments to derive water correction coefficients for the application to the complete Ambarchik record.

Revision 2.9.2019 11:07
Gelöscht: (2018).

Experiments were performed with two different humidification methods. For the so-called droplet method, a droplet of de-ionized water (ca. 1 ml) was injected into the dry air stream from a pressurized air tank and measured with the CRDS analyzer. The gradual evaporation of the droplet provided varying water vapor levels. By contrast to the droplet method, the gas washing bottle method was designed to hold water content in the sampled air at stable levels. For this purpose, the air stream from a pressurized tank was humidified by directing it through a gas washing bottle filled with de-ionized water, resulting in an air stream saturated with water vapor. The humid air was mixed with a second, untreated air stream from the same tank. Different water vapor levels were realized by varying the relative flow through the lines using needle valves.

Initial experiments have been performed using the droplet method, but systematic biases in the resulting dry air mole fractions at $H_2O < 0.5$ % led to further experiments with the gas washing bottle method and the development of an improved water correction model:

$$f_c(\boldsymbol{h}) = \underbrace{\boldsymbol{1 + a_c \cdot h + b_c \cdot h^2}}_{f_c^{para}(\boldsymbol{h})} + \boldsymbol{d_c} \cdot \left(\boldsymbol{e^{-\frac{h}{h_p}} - 1} \right) \quad \textbf{(B.1)}$$

Here, $\boldsymbol{f_c^{para}(h)}$ corrects for dilution and pressure broadening (Chen et al., 2010). The parameters d_c and h_p correct for a sensitivity of pressure inside the measurement cavity of Picarro analyzers to water vapor (Reum et al., 2019).

Three droplet experiments were performed in 2014, while one gas washing bottle experiment was performed in each 2015 and 2017. The droplet results proved unsuitable to derive the pressure-related coefficients $\boldsymbol{d_c}$ and $\boldsymbol{h_p}$ due to fast variations of water vapor, which typically occurred below 0.5 % H_2O (Reum et al., 2019). Therefore, from the droplet experiments only the data with slowly varying water vapor were used, and $\boldsymbol{d_c}$ and $\boldsymbol{h_p}$ were based only on the gas washing bottle experiments. For each species, a synthesis water correction function was derived by fitting coefficients to the average response of the individual functions (Table B.1).

Revision 2.9.2019 11:07
Gelöscht: 2018

Revision 2.9.2019 11:07
Gelöscht: method

Revision 2.9.2019 11:07
Gelöscht: (Reum et al., 2018).

Table B.1: Synthesis water correction coefficients. Uncertainties are approximated by the maximum difference between the coefficients of the individual water correction functions and the coefficient of synthesis function.

Species	a_c [(% H_2O_{rep})$^{-1}$]	b_c [(% H_2O_{rep})$^{-2}$]	d_c [unitless]	h_p [% H_2O_{rep}]

CO_2	$(-1.2 \pm 0.2) \times 10^{-2}$	$(-2.7 \pm 0.5) \times 10^{-4}$	$(2.2 \pm 1.0) \times 10^{-4}$	0.22 ± 0.12
CH_4	$(-0.97 \pm 0.07) \times 10^{-2}$	$(-3.1 \pm 1.4) \times 10^{-4}$	$(1.1 \pm 0.7) \times 10^{-3}$	0.22 ± 0.12

Appendix C Calibration scale and coefficients

Table C.1: Calibrated dry air mole fractions of the air tanks in use at Ambarchik over the period covered in this paper. For a discussion of the uncertainties, see Appendix E.2.

Name	WMO scale X2007 CO_2 [ppm]	WMO scale X2004A CH_4 [ppb]
High Tank	444.67 ± 0.03	2366.95 ± 0.31
Middle Tank	398.68 ± 0.03	1962.39 ± 0.31
Low Tank	354.37 ± 0.03	1796.94 ± 0.31
Target Tank	401.56 ± 0.03	1941.96 ± 0.31

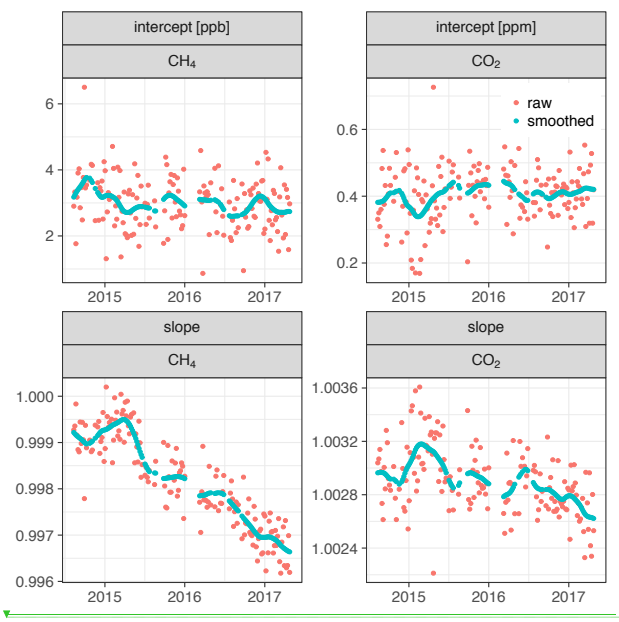

Fig. C.1: Coefficients of linear fits to High, Middle and Low Tank. The smoothed coefficients are used for calibrating data.

Revision 2.9.2019 11:07

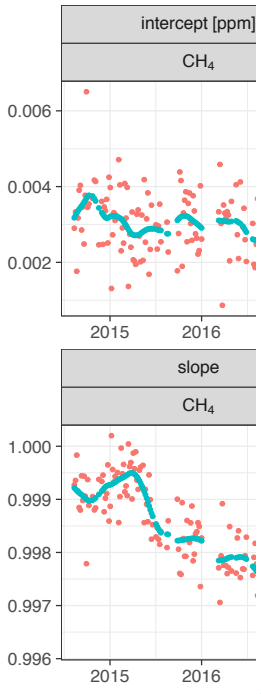

Gelöscht:

Appendix D Spike detection algorithm for CO_2

The CO_2 spike detection algorithm is a multi-step process. First, candidates for CO_2 spikes are identified. In subsequent steps, false positives are removed. Parts of the algorithm are based on Vickers and Mahrt (1997).

Step 1. Identifying spike candidates based on variation of differences between CO_2 measurements

For this step, data are processed in intervals spanning 1.5 hours. Candidates for CO_2 spikes are identified based on the variability of differences between individual consecutive CO_2 measurements. Measurements with differences that exceed 3.5 standard deviations from non-flagged data are flagged as spike candidates. Since flagging the data changes the standard deviation of the non-flagged data, flagging is repeatedly applied until changes between standard deviations of the non-flagged data between the last and second-last loop are less than 10^{-10} ppm CO_2. In some cases, this procedure flags the complete interval as spikes. This happens when the variations throughout the interval are rather uniform. This might be the case both in the presence of spikes throughout the interval, or absence of spikes altogether. To avoid false positives, all flags are removed, and the interval is considered to have no spikes. Cases with many spikes throughout the interval can be filtered based on the intra-hour variability flag.

Revision 2.9.2019 11:07
Gelöscht: when all CO_2 data in the interval have rather uniform variations

Revision 2.9.2019 11:07
Gelöscht: whole interval. In that

Step 2. Blurring

Around the top of a spike, differences between individual CO_2 soundings are often small and thus, these measurements are not captured as part of a spike in step 1. To unite the ascending and descending parts of spikes, the 20 data points before and after a flagged measurement are flagged. From here on, each group of consecutive flagged measurements is considered a spike candidate.

Step 3. Unflagging individual outliers

Step one often identifies individual or very few consecutive data points as spikes, spanning few seconds. We regard these very small groups of flagged data points as noise misidentified as spikes. After blurring (step 2), these individual outliers form groups of at least 41 data points. In step 3, spike candidates consisting of less than 45 data points are unflagged.

Step 4. Baseline, detrending

For each spike candidate, the baseline is identified as a linear fit to the unflagged measurements within five minutes of any data point of the spike candidate. Using this baseline, the data in this interval are detrended, including the spike candidate.

Step 5. Spike height

From the detrended data from step 4, the maximum deviation from the baseline ("spike height") is calculated. Spike candidates smaller than 8 standard deviations of the baseline measurements are unflagged.

Step 6. Unflagging abrupt but persistent changes

Until the previous step, the algorithm flags abrupt CO_2 changes even if they are persistent. This pattern occurs for example during changes of wind direction and does not constitute an isolated spike. In this case, a trough is present in the detrended spike. The minimum deviation from the baseline is calculated ("trough depth") and compared to the spike height. Since spike height and trough depths can be based on few data points, the influence of noise is strong. To counteract, spike height and trough depth are diminished by two standard deviations of the baseline. Spike candidates with trough depths greater than one fifth of the spike height are unflagged.

Step 7. Unflagging persistent variability changes

The procedure so far can flag the beginning or end of longer periods of larger CO_2 variability. To unflag these false positives, steps 4–5 are applied again with the following changes: (1) a longer baseline of 30 minutes before and after the spike candidate (instead of five minutes) is used, (2) baseline standard deviations are calculated separately for the period before and after the spike candidate, (3) the spike height from step 5 is used instead of recalculated, and (4) the spike height must exceed the maximum of the two baseline standard deviations by a factor of 6 instead of 8.

Step 8. Repeat

The result from steps 4–7 depends on unflagged data points surrounding a spike candidate. Therefore, these steps are repeated until a steady state is reached.

An example of flagged spikes is shown in Fig. D.1. In this example, removing flagged data reduced the hourly averages of Center inlet data between 3 and 4 a.m. by 0.5 ppm (CO_2) and 7.0 ppb (CH_4). No Top

inlet data were flagged in this period. Since small spikes can be hard to distinguish from natural signals, some smaller features can pass the algorithm without being flagged that may be classified as spikes upon visual inspection, e.g. at 5:33 a.m. in Fig. D.1. However, given that larger spikes alter hourly averages by values on the order of magnitude of the WMO goals, the impact of these features is likely negligible. In this particular example, removing the detected spikes reduced average CO_2 mole fractions between 5 and 6 a.m. from the Center inlet by 0.07 ppm. Removing the unflagged small spike at 5:33 a.m. would further reduce this average by 0.005 ppm, which is inconsequential.

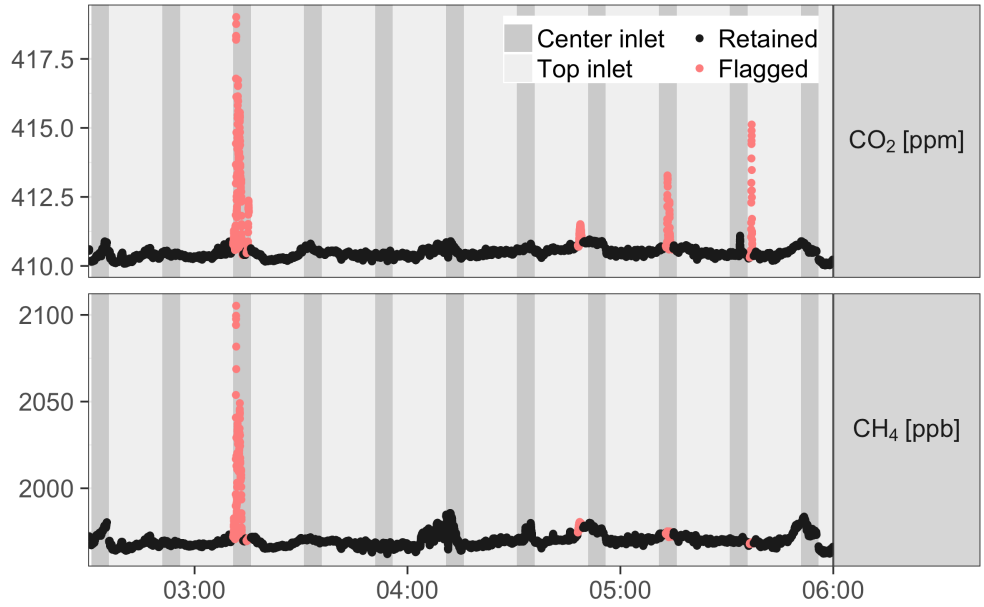

Fig. D.1: Example of a series of flagged CO_2 spikes from December 4, 2016.

Appendix E Measurement uncertainties

We adopted the uncertainty quantification method of Andrews et al. (2014). Here, we summarize the main ideas of this approach, the modifications we made, and quantify individual uncertainty

components. A detailed description of the nomenclature and method was omitted; please refer to Andrews et al. (2014).

E.1 Uncertainty estimation framework by Andrews et al. (2014) and modifications

Andrews et al. (2014) calculated the measurement uncertainty as the largest of four different formulations (Eq. (9a–d) therein). Formulations (a) and (b) were the prediction interval of the linear regression of the calibration tanks, which takes into account the standard error of the fit (se_{fit}) and the uncertainty in the analyzer signal. The difference between (a) and (b) was the estimate of the uncertainty in the analyzer signal. In formulation (a), it was estimated from a model (σ_u) that accounts for analyzer precision (u_p) and drift (u_b), uncertainty of the water vapor correction (u_{wv}), equilibration after switching calibration tanks (u_{eq}) and extrapolation beyond the range covered by the calibration tanks (u_{ex}). In measurement uncertainty formulation (b), the uncertainty estimate of the analyzer signal was estimated from the residuals of the linear fits of the calibration tank mole fractions (σ_y), accounting for the fact that the assigned values of the calibration tanks have non-zero uncertainty (σ_x):

$$\sigma'_y = \sqrt{{\sigma_y}^2 - (m\sigma_x)^2} \quad \textbf{(E.1)}$$

Here, m is the slope of the calibration function. Formulation (c) was the bias of the Target tank (u_{TGT}), and formulation (d) the uncertainty in the assigned values of the calibration tanks (σ_x). In this approach, uncertainty formulations (b), (c) and (d) only accounted for uncertainties of dry air measurements. Hence, we modified it by adding the uncertainty of the water correction to these formulations. Thus, the analyzer precision model for uncertainty formulation (a) became:

$$\sigma_u = \sqrt{{u_p}^2 + {u_b}^2 + {u_{eq}}^2 + {u_{ex}}^2} \quad \textbf{(E.2)}$$

The full uncertainty terms were thus:

$$u_{M,a} = \sqrt{\left(z_{(\alpha,f)}\right)^2 \left(\frac{se_{fit}}{m}\right)^2 + {\sigma_u}^2 + {u_{wv}}^2} \quad \textbf{(E.3)}$$

$$u_{M,b} = \sqrt{\left(z_{(\alpha,f)}\right)^2 \left(\left(\frac{se_{fit}}{m}\right)^2 + \left(\frac{\sigma'_y}{m}\right)^2 \right) + {u_{wv}}^2} \quad \text{(E.4)}$$

$$u_{M,c} = \sqrt{{u_{TGT}}^2 + {u_{wv}}^2} \quad \text{(E.5)}$$

$$u_{M,d} = \sqrt{{\sigma_x}^2 + {u_{wv}}^2} \quad \text{(E.6)}$$

Here, $z_{(\alpha,f)}$ is a factor based on the quantile function of Student's t distribution with confidence level α ($\alpha = 0.675$ for prediction interval at 1σ-level) and degrees of freedom f. Calibration uncertainties were estimated based on the averaging strategy for coefficients, i.e., using linear fits of weighted observations from individual calibration episodes over a window of 120 days (Sect. 3.2), which usually contained about 25 calibration episodes. The standard error of the fit (se_{fit}) was computed based on these weighted fits. In the notation of Andrews et al., (2014), the equations for se_{fit} become (cf. Taylor, 1997):

$$se_{fit} = \sqrt{\left(\sigma_m (x - \bar{x})\right)^2 + {\sigma_{bmin}}^2} \quad \text{(E.7)}$$

$$\sigma_m = \frac{\sigma_y}{\sqrt{\sum w_i (x_i - \bar{x})^2}} \quad \text{(E.8)}$$

$$\sigma_{bmin} = \sigma_y \sqrt{\frac{\sum w_i (x_i - \bar{x})^2}{(\sum w_i) \sum w_i (x_i - \bar{x})^2 - (\sum w_i (x_i - \bar{x}))^2}} \quad \text{(E.9)}$$

$$\sigma_y = \sqrt{\frac{\sum w_i \left(y_i - y_{i,fit}\right)^2}{df}} \quad \text{(E.10)}$$

Here, all quantities are as in Andrews et al., (2014), with the addition of weights w_i and degrees of freedom df, which change with the number of calibration episodes in an interval.

Compared to calibrating based on single calibration episodes, this affected the uncertainty because of the larger number of observations (reduction of se_{fit} and $z_{(\alpha,f)}$), and because of drift of the analyzer signal over the averaging window (increase of se_{fit} and σ'_y).

Revision 2.9.2019 11:07

Gelöscht: Here, $z_{(\alpha,f)}$ is the quantile function of Student's t distribution. At Ambarchik, three calibration tanks are used to infer linear calibration functions. Thus, for a prediction interval at 1σ-level, $z_{(\alpha=0.675,f=1)} = 1.79$.

E.2 Uncertainty components and estimates

In the following paragraphs, the individual components of the four uncertainty estimates Eq. (E.3)–(E.6) are described. For numerical values of the components, see Table E.1. The time-varying uncertainty estimates $u_{M,a-d}$ are shown in Fig. E.1.

Water-vapor (u_{wv})

For the water correction uncertainty u_{wv}, we used the maximum of the difference between individual water correction functions and the synthesis water correction function, i.e. 0.018 % CO_2 and 0.034 % CH_4, regardless of actual water content. This approach likely overestimates u_{wv} at low water vapor content, but was chosen because u_{wv} was not well constrained by the small number of water correction experiments conducted so far.

Assigned values of calibration gas tanks (σ_x)

For the uncertainty of the assigned values of the calibration gas tanks σ_x, we followed the approach by Andrews et al. (2014), who set them to the reproducibility of the primary scales WMO X2007 (CO_2) and WMO X2004 (CH_4). Estimates based on the MPI-BGC implementations of the primary scales yielded smaller uncertainties that underestimated the mismatch between the CO_2 mole fractions of the calibration tanks.

Target tank (u_{TGT})

The uncertainty based on the Target tank measurements u_{TGT} was the same as in Andrews et al. (2014), but with the weighting and window we used for smoothing the calibration coefficients.

Analyzer signal precision model (σ_u)

For the analyzer signal precision model σ_u, analyzer precision (u_p) and drift (u_b) were estimated jointly ($\sqrt{{u_p}^2 + {u_b}^2}$) as the standard deviation of hourly averages of a gas tank measurement over 12 days prior to field deployment. Note that se_{fit} also accounts for drift of the analyzer signal. However, the contribution of drift on timescales significantly shorter than the averaging window of 120 days to se_{fit} tends toward zero. Since the estimate of u_b was based on 12 days of measurements, it represents drift over this shorter time scale in the prediction interval, which is why it was included in the model. The other components (σ_{eq}, σ_{ex}) appeared negligible. In particular, we found no conclusive evidence of

Revision 2.9.2019 11:07
Gelöscht: from variations during a gas tank measurement over 12 days prior to field deployment.

non-negligible equilibration errors (σ_{eq}) in our calibrations; however, this remains subject of future research (Appendix E.4). The extrapolation uncertainty (σ_{ex}) applied only to a small fraction of Ambarchik data, so we ignored this error.

Table E.1: Measurement uncertainty components. The nomenclature follows Andrews et al. (2014). For time-varying components, averages are reported and denoted with an asterisk (*).

Uncertainty component	CO_2 [ppm]	CH_4 [ppb]
Water correction u_{wv}	* 0.075	* 0.67
Assigned values of calibration gas tanks σ_x	0.03	0.31
Analyzer signal (a) σ_u	0.013	0.25
Analyzer signal (b) σ'_y	* 0.018	* 0.17
Standard error of fit se_{fit}	* 0.005	* 0.05
Target tank deviation from laboratory value u_{TGT}	* 0.038	* 0.32
Maximum of estimates $u_{M,a–d}$	* 0.085	* 0.77

Revision 2.9.2019 11:07
Gelöscht: to

Revision 2.9.2019 11:07
Gelöscht: 058

Revision 2.9.2019 11:07
Gelöscht: 00

Revision 2.9.2019 11:07
Gelöscht: 047

Revision 2.9.2019 11:07
Gelöscht: 11

Revision 2.9.2019 11:07
Gelöscht: 11

Revision 2.9.2019 11:07
Gelöscht: 75

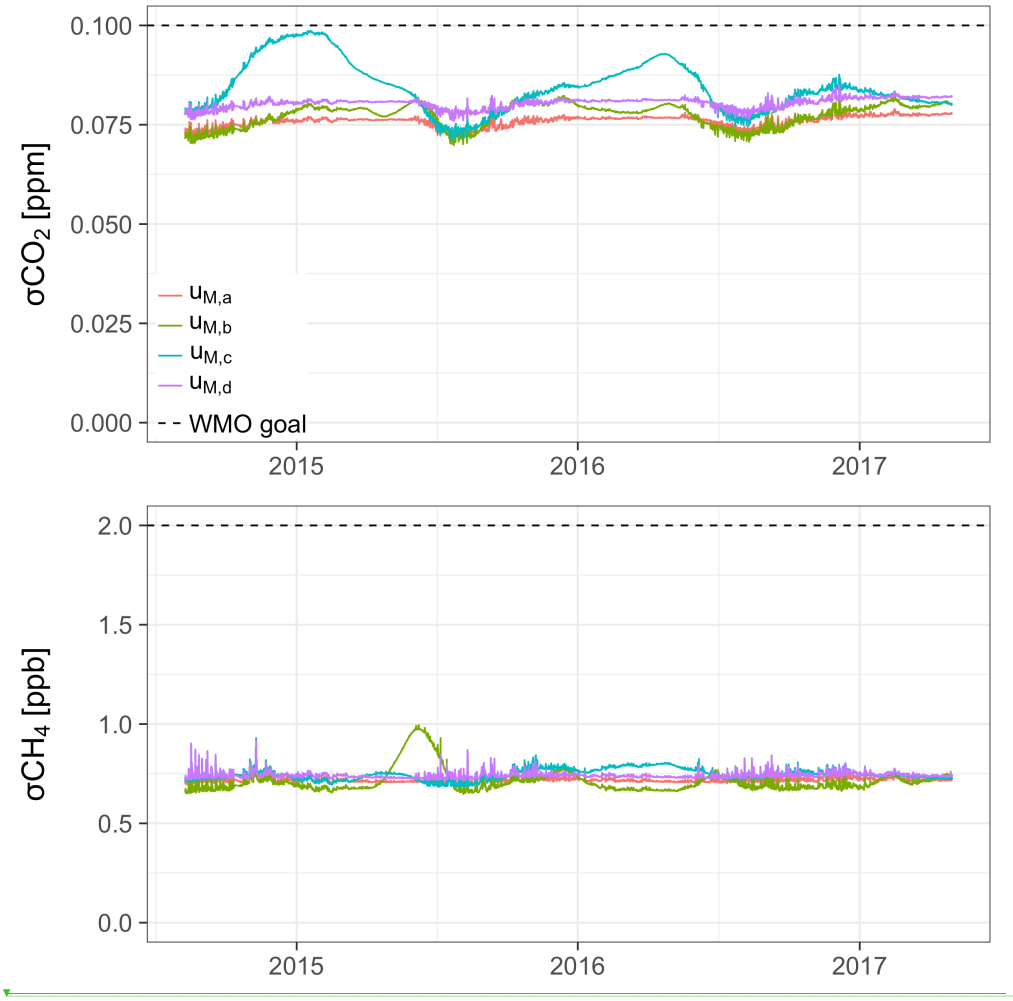

Revision 2.9.2019 11:07

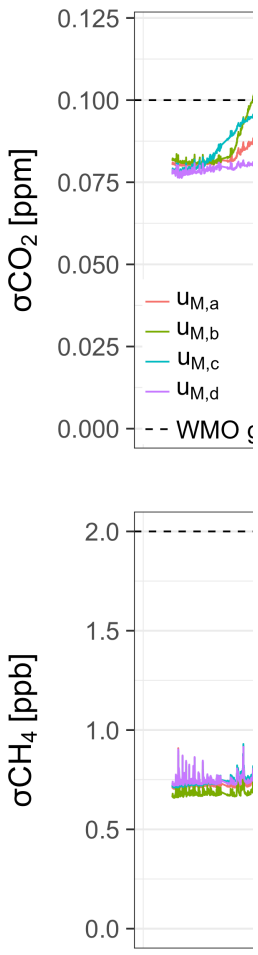

Gelöscht:

Fig. E.1: Estimates of CO_2 and CH_4 measurement uncertainty as defined in Eq. (E.3)–(E.6). The dashed lines are the WMO inter-laboratory compatibility goals.

E.3 Random and systematic uncertainty components

The uncertainty components described in Sect. E.1 and E.2 are mostly independent of the averaging period for which atmospheric data are reported (one hour). Rather, they describe systematic uncertainties inherent to the calibration procedure and long-term drift (σ_x, se_{fit}, u_{TGT}), and the water correction (u_{wv}). Thus, these uncertainty estimates would not be smaller for atmospheric data averaged over longer periods. Exceptions are the analyzer signal precision estimates σ_u and σ'_y, which contain random uncertainties: the precision model σ_u was estimated based on hourly averages and reflects both their uncertainty and drift on the timescale of 12 days. Thus, it might change for different averaging periods. The analyzer signal uncertainty estimate σ'_y was sensitive to several timescales, i.e., two minutes (averaging period of calibration data), 22 minutes (timespan of data of one calibration episode), 116 hours (time between individual calibration episodes) and 120 days (averaging window for calibration coefficients). To investigate whether uncertainties at these timescales were similar to those of the hourly averages of atmospheric data, we computed the Allan deviations for CO_2 and CH_4. The uncertainties of averages over two minutes, 22 minutes and one hour were close (Fig. E.2). In addition, the analyzer precision deteriorated beyond one hour. These results are similar (qualitatively and quantitatively) to those documented by Yver Kwok et al. (2015) for several Picarro GHG analyzers.

The analyzer signal precision estimates accounted for only a small fraction of the total uncertainty (Table E.1). Thus, the random uncertainty components play a minor role in the calibration of Ambarchik data, and averaging atmospheric data over different periods would not change the total estimated uncertainty considerably.

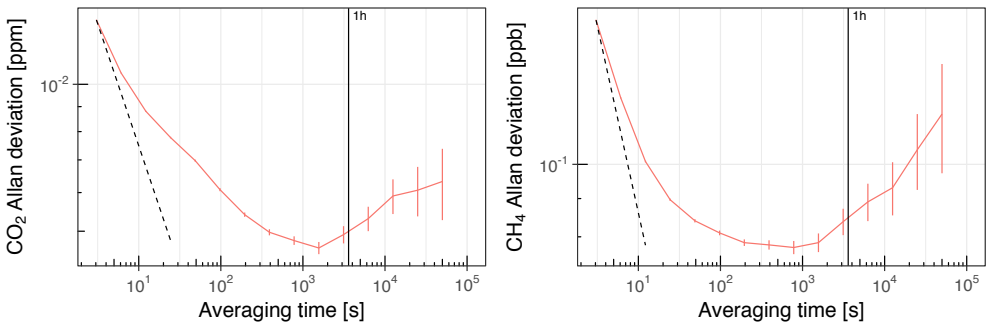

Fig. E.2: Allan deviation of the CO_2 and CH_4 readings of the CRDS analyzer in Ambarchik. Values are based on one 12-day measurement of dry air from a gas tank in the lab prior to field deployment. The averaging time is cut off where the error gets too large for a meaningful interpretation of the result. The vertical line denotes an averaging time of one hour. The dashed line corresponds to white noise (slope -0.5), scaled to coincide with the first data point of the Allan deviation.

E.4 Potential improvements of the calibration accuracy

Several aspects to the accuracy of the calibration using regular gas tank measurements are subject to future research. Here, we outline potential calibration errors that could not be conclusively quantified, and how we plan to address them in the future.

To investigate whether the regular probing time of the gas tanks was sufficient for equilibration (e.g. due to flushing of the tubing), we fitted exponential functions to the medians of the regular tank measurements. Deviations between modeled equilibrium mole fractions and the averages used for calibration were negligible ($|\Delta CO_2| < 0.008$ ppm; $|\Delta CH_4| < 0.09$ ppb) and thus ignored. Furthermore, in two experiments, we investigated equilibration error and other drifts (e.g. diffusion in the pressure reducers) by measuring the calibration tanks in reversed order, and in original order for up to two hours. However, the experiments were inconclusive. Based on the available data, we estimated the largest conceivable biases for the ranges 350–450 ppm CO_2 and 1800–2400 ppb CH_4. They were up to 0.06 ppm CO_2 and 0.5 ppb CH_4 at the edges of these ranges and vanished around their centers. An additional source of bias might be inlet pressure sensitivity of the Picarro analyzer as documented by Gomez-Pelaez et al. (2019). Using the sensitivities reported therein, some of the gas tank measurements in

Revision 2.9.2019 11:07
Gelöscht: More experiments are necessary to

Ambarchik could have a bias of up to 0.03 ppm CO_2 and 0.2 ppb CH_4. More experiments are necessary to rule out or confirm and assess these possible biases; hence, no bias correction was implemented.

The CO_2 bias of the water-corrected Target tank mole fractions varied from -0.06 to -0.01 ppm (Fig. 5, left). These variations correlated with residual water vapor (which was much smaller than 0.01 %) and temperature in the laboratory during the Target tank measurements, as well as with ambient CO_2 mole fractions sampled before. This suggests that the variations may be due to insufficient flushing during calibration. However, the correlations varied over time without changes to the hardware or probing strategy. Therefore, further investigation of this observation is required, and no correction was implemented.

So far, possible drifts of the gas tanks could not be assessed and have thus not been included in our uncertainty assessment. This will be assessed only when the gas tanks are almost empty, and shipped back to the MPI-BGC for recalibration.

Data availability

Quality-controlled hourly averages of data from Ambarchik are available on request from Mathias Göckede. We plan to publish continuous updates to the data to an open access repository in the future.

Author contributions

MH, SZ and MG conceptualized the study. JL, MH, OK, NZ, FR and MG designed and set up the Ambarchik station. NZ and SZ coordinated setup and maintenance of the Ambarchik station. FR and MP performed calibration experiments. FR curated and analyzed the data. FR prepared the manuscript with contributions from all authors. MG supervised the project, and reviewed and edited the manuscript.

Competing interests

The authors declare that they have no conflict of interest.

Acknowledgements

This work was supported by the Max-Planck Society, the European Commission (PAGE21 project, FP7-ENV-2011, grant agreement No. 282700; PerCCOM project, FP7-PEOPLE-2012-CIG, grant agreement No. PCIG12-GA-201-333796; INTAROS project, H2020-BG-2016-2017, grant agreement No. 727890), the German Ministry of Education and Research (CarboPerm-Project, BMBF grant No. 03G0836G), the AXA Research Fund (PDOC_2012_W2 campaign, ARF fellowship M. Göckede), and the European Science Foundation (TTorch Research Networking Programme, Short Visit Grant F. Reum). The authors would like to thank Armin Jordan (MPI-BGC) for preparing the gas cylinders. We would also like to thank C. Rödenbeck (MPI-BGC) for access to the Jena Inversion code for producing global CO_2 mole fraction fields, T. Nunez-Ramirez (MPI-BGC) for providing global CH_4 mole fraction fields and John Henderson (AER) for providing footprints for Ambarchik.

Revision 2.9.2019 11:07
Gelöscht: T.

References

Andrews, A. E., Kofler, J. D., Trudeau, M. E., Williams, J. C., Neff, D. H., Masarie, K. A., Chao, D. Y., Kitzis, D., Novelli, P. C., Zhao, C. L., Dlugokencky, E. J., Lang, P. M., Crotwell, M. J., Fischer, M. L., Parker, M. J., Lee, J. T., Baumann, D. D., Desai, A. R., Stanier, C. O., De Wekker, S. F. J., Wolfe, D. E., Munger, J. W. and Tans, P. P.: CO_2, CO, and CH_4 measurements from tall towers in the NOAA earth system research laboratory's global greenhouse gas reference network: Instrumentation, uncertainty analysis, and recommendations for future high-accuracy greenhouse gas, Atmos. Meas. Tech., 7(2), 647–687, doi:10.5194/amt-7-647-2014, 2014.

Belshe, E. F., Schuur, E. A. G. and Bolker, B. M.: Tundra ecosystems observed to be CO_2 sources due to differential amplification of the carbon cycle., Ecol. Lett., 16(10), 1307–15, doi:10.1111/ele.12164, 2013.

Berchet, A., Bousquet, P., Pison, I., Locatelli, R., Chevallier, F., Paris, J.-D., Dlugokencky, E. J., Laurila, T., Hatakka, J., Viisanen, Y., Worthy, D. E. J., Nisbet, E. G., Fisher, R., France, J., Lowry, D., Ivakhov, V. and Hermansen, O.: Atmospheric constraints on the methane emissions from the East Siberian Shelf, Atmos. Chem. Phys., 16(6), 4147–4157, doi:10.5194/acp-16-4147-2016, 2016.

Chen, H., Winderlich, J., Gerbig, C., Hoefer, A., Rella, C. W., Crosson, E. R., Van Pelt, A. D., Steinbach, J., Kolle, O., Beck, V., Daube, B. C., Gottlieb, E. W., Chow, V. Y., Santoni, G. W. and Wofsy, S. C.: High-accuracy continuous airborne measurements of greenhouse gases (CO_2 and CH_4) using the cavity ring-down spectroscopy (CRDS) technique, Atmos. Meas. Tech., 3(2), 375–386, doi:10.5194/amt-3-375-2010, 2010.

Danielson, J. J. and Gesch, D. B.: Global Multi-resolution Terrain Elevation Data 2010 (GMTED2010), U.S. Geol. Surv. Open-File Rep. 2011–1073, 2010, 26, 2011.

Dlugokencky, E. J., Crotwell, A. M., Lang, P. M. and Mund, J. W.: Atmospheric Methane Dry Air Mole Fractions from quasi-continuous measurements at Barrow, Alaska and Mauna Loa, Hawaii, 1986-2016, Version: 2017-01-20, [online] Available from: ftp://aftp.cmdl.noaa.gov/data/trace_gases/ch4/in-situ/surface, 2017.

Euskirchen, E. S., Bret-Harte, M. S., Scott, G. J., Edgar, C. and Shaver, G. R.: Seasonal patterns of carbon dioxide and water fluxes in three representative tundra ecosystems in northern Alaska, Ecosphere, 3(1), 1–19, doi:10.1890/ES11-00202.1, 2012.

Gomez-Pelaez, A. J., Ramos, R., Cuevas, E., Gomez-Trueba, V. and Reyes, E.: Atmospheric CO_2, CH_4, and CO with the CRDS technique at the Izaña Global GAW station: instrumental tests, developments, and first measurement results, Atmos. Meas. Tech., 12(4), 2043–2066, doi:10.5194/amt-12-2043-2019, 2019.

Goodrich, J. P., Oechel, W. C., Gioli, B., Moreaux, V., Murphy, P. C., Burba, G. and Zona, D.: Impact of different eddy covariance sensors, site set-up, and maintenance on the annual balance of CO_2 and CH_4 in the harsh Arctic environment, Agric. For. Meteorol., 228–229, 239–251, doi:10.1016/j.agrformet.2016.07.008, 2016.

Henderson, J. M., Eluszkiewicz, J., Mountain, M. E., Nehrkorn, T., Chang, R. Y.-W., Karion, A., Miller, J. B., Sweeney, C., Steiner, N., Wofsy, S. C. and Miller, C. E.: Atmospheric transport simulations in support of the Carbon in Arctic Reservoirs Vulnerability Experiment (CARVE), Atmos. Chem. Phys., 15(8), 4093–4116, doi:10.5194/acp-15-4093-2015, 2015.

Hugelius, G., Strauss, J., Zubrzycki, S., Harden, J. W., Schuur, E. A. G., Ping, C. L., Schirrmeister, L., Grosse, G., Michaelson, G. J., Koven, C. D., O'Donnell, J. A., Elberling, B., Mishra, U., Camill, P., Yu,

Z., Palmtag, J. and Kuhry, P.: Estimated stocks of circumpolar permafrost carbon with quantified uncertainty ranges and identified data gaps, Biogeosciences, 11(23), 6573–6593, doi:10.5194/bg-11-6573-2014, 2014.

IPCC: Climate Change 2013. The Physical Science Basis. Working Group 1 Contribution to the Fifth Assessment Report of the Intergovernmental Panel on Climate Change., 2013.

James, R. H., Bousquet, P., Bussmann, I., Haeckel, M., Kipfer, R., Leifer, I., Niemann, H., Ostrovsky, I., Piskozub, J., Rehder, G., Treude, T., Vielstädte, L. and Greinert, J.: Effects of climate change on methane emissions from seafloor sediments in the Arctic Ocean: A review, Limnol. Oceanogr., 61(S1), S283–S299, doi:10.1002/lno.10307, 2016.

Jeong, S.-J., Bloom, A. A., Schimel, D., Sweeney, C., Parazoo, N. C., Medvigy, D., Schaepman-Strub, G., Zheng, C., Schwalm, C. R., Huntzinger, D. N., Michalak, A. M. and Miller, C. E.: Accelerating rates of Arctic carbon cycling revealed by long-term atmospheric CO_2 measurements, Sci. Adv., 4(7), eaao1167, doi:10.1126/sciadv.aao1167, 2018.

Kittler, F., Burjack, I., Corradi, C. A. R., Heimann, M., Kolle, O., Merbold, L., Zimov, N., Zimov, S. A. and Göckede, M.: Impacts of a decadal drainage disturbance on surface–atmosphere fluxes of carbon dioxide in a permafrost ecosystem, Biogeosciences, 13(18), 5315–5332, doi:10.5194/bg-13-5315-2016, 2016.

Kittler, F., Eugster, W., Foken, T., Heimann, M., Kolle, O. and Göckede, M.: High-quality eddy-covariance CO_2 budgets under cold climate conditions, J. Geophys. Res. Biogeosciences, 122(8), 2064–2084, doi:10.1002/2017JG003830, 2017a.

Kittler, F., Heimann, M., Kolle, O., Zimov, N., Zimov, S. A. and Göckede, M.: Long-Term Drainage Reduces CO_2 Uptake and CH_4 Emissions in a Siberian Permafrost Ecosystem, Global Biogeochem. Cycles, 31(12), 1704–1717, doi:10.1002/2017GB005774, 2017b.

Kwon, M. J., Beulig, F., Ilie, I., Wildner, M., Küsel, K., Merbold, L., Mahecha, M. D., Zimov, N., Zimov, S. A., Heimann, M., Schuur, E. A. G., Kostka, J. E., Kolle, O., Hilke, I. and Göckede, M.: Plants, microorganisms, and soil temperatures contribute to a decrease in methane fluxes on a drained Arctic floodplain, Glob. Chang. Biol., 23(6), 2396–2412, doi:10.1111/gcb.13558, 2017.

Lin, J. C., Gerbig, C., Wofsy, S. C., Andrews, A. E., Daube, B. C., Davis, K. J. and Grainger, C. A.: A

near-field tool for simulating the upstream influence of atmospheric observations: The Stochastic Time-Inverted Lagrangian Transport (STILT) model, J. Geophys. Res., 108(D16), 4493, doi:10.1029/2002JD003161, 2003.

Masarie, K. A., Pétron, G., Andrews, A. E., Bruhwiler, L., Conway, T. J., Jacobson, A. R., Miller, J. B., Tans, P. P., Worthy, D. E. J. and Peters, W.: Impact of CO_2 measurement bias on CarbonTracker surface flux estimates, J. Geophys. Res. Atmos., 116(17), 1–13, doi:10.1029/2011JD016270, 2011.

Mastepanov, M., Sigsgaard, C., Dlugokencky, E. J., Houweling, S., Ström, L., Tamstorf, M. P. and Christensen, T. R.: Large tundra methane burst during onset of freezing., Nature, 456(7222), 628–30, doi:10.1038/nature07464, 2008.

Mastepanov, M., Sigsgaard, C., Tagesson, T., Ström, L., Tamstorf, M. P., Lund, M. and Christensen, T. R.: Revisiting factors controlling methane emissions from high-Arctic tundra, Biogeosciences, 10(11), 5139–5158, doi:10.5194/bg-10-5139-2013, 2013.

McGuire, A. D., Christensen, T. R., Hayes, D., Heroult, A., Euskirchen, E. S., Kimball, J. S., Koven, C. D., Lafleur, P., Miller, P. A., Oechel, W. C., Peylin, P., Williams, M. R. and Yi, Y.: An assessment of the carbon balance of Arctic tundra: comparisons among observations, process models, and atmospheric inversions, Biogeosciences, 9(8), 3185–3204, doi:10.5194/bg-9-3185-2012, 2012.

Miller, S. M., Worthy, D. E. J., Michalak, A. M., Wofsy, S. C., Kort, E. A., Havice, T. C., Andrews, A. E., Dlugokencky, E. J., Kaplan, J. O., Levi, P. J., Tian, H. and Zhang, B.: Observational constraints on the distribution, seasonality, and environmental predictors of North American boreal methane emissions, Global Biogeochem. Cycles, 28(2), 146–160, doi:10.1002/2013GB004580, 2014.

NOAA: Atmospheric Carbon Dioxide Dry Air Mole Fractions from quasi-continuous measurements at Barrow, Alaska. Compiled by K.W. Thoning, D.R. Kitzis, and A. Crotwell. National Oceanic and Atmospheric Administration (NOAA), Earth System Research Laboratory (ESRL)., 2015.

Oechel, W. C., Laskowski, C. A., Burba, G., Gioli, B. and Kalhori, A. A. M.: Annual patterns and budget of CO_2 flux in an Arctic tussock tundra ecosystem, J. Geophys. Res. Biogeosciences, 119(3), 323–339, doi:10.1002/2013JG002431, 2014.

Olson, D. M., Dinerstein, E., Wikramanayake, E. D., Burgess, N. D., Powell, G. V. N., Underwood, E. C., D'amico, J. A., Itoua, I., Strand, H. E., Morrison, J. C., Loucks, C. J., Allnutt, T. F., Ricketts, T. H.,

Revision 2.9.2019 11:07
Gelöscht: ACH 2-1-ACH 2-17

Kura, Y., Lamoreux, J. F., Wettengel, W. W., Hedao, P. and Kassem, K. R.: Terrestrial Ecoregions of the World: A New Map of Life on Earth, Bioscience, 51(11), 933, doi:10.1641/0006-3568(2001)051[0933:TEOTWA]2.0.CO;2, 2001.

Park, T., Ganguly, S., Tømmervik, H., Euskirchen, E. S., Høgda, K.-A., Karlsen, S. R., Brovkin, V., Nemani, R. R. and Myneni, R. B.: Changes in growing season duration and productivity of northern vegetation inferred from long-term remote sensing data, Environ. Res. Lett., 11(8), 84001, doi:10.1088/1748-9326/11/8/084001, 2016.

Peters, W., Krol, M. C., van der Werf, G. R., Houweling, S., Jones, C. D., Hughes, J., Schaefer, K., Masarie, K. A., Jacobson, A. R., Miller, J. B., Cho, C. H., Ramonet, M., Schmidt, M., Ciattaglia, L., Apadula, F., Heltai, D., Meinhardt, F., di Sarra, A. G., Piacentino, S., Sferlazzo, D., Aalto, T., Hatakka, J., Ström, J., Haszpra, L., Meijer, H. A. J., van Der Laan, S., Neubert, R. E. M., Jordan, A., Rodó, X., Morguí, J. A., Vermeulen, A. T., Popa, E., Rozanski, K., Zimnoch, M., Manning, A. C., Leuenberger, M., Uglietti, C., Dolman, A. J., Ciais, P., Heimann, M. and Tans, P. P.: Seven years of recent European net terrestrial carbon dioxide exchange constrained by atmospheric observations, Glob. Chang. Biol., 16(4), 1317–1337, doi:10.1111/j.1365-2486.2009.02078.x, 2010.

Rella, C. W., Chen, H., Andrews, A. E., Filges, A., Gerbig, C., Hatakka, J., Karion, A., Miles, N. L., Richardson, S. J., Steinbacher, M., Sweeney, C., Wastine, B. and Zellweger, C.: High accuracy measurements of dry mole fractions of carbon dioxide and methane in humid air, Atmos. Meas. Tech., 6(3), 837–860, doi:10.5194/amt-6-837-2013, 2013.

Reum, F., Gerbig, C., Lavric, J. V, Rella, C. W. and Göckede, M.: Correcting atmospheric CO_2 and CH_4 mole fractions obtained with Picarro analyzers for sensitivity of cavity pressure to water vapor, Atmos. Meas. Tech., 12(2), 1013–1027, doi:10.5194/amt-12-1013-2019, 2019.

Rienecker, M. M., Suarez, M. J., Gelaro, R., Todling, R., Bacmeister, J., Liu, E., Bosilovich, M. G., Schubert, S. D., Takacs, L., Kim, G. K., Bloom, S., Chen, J., Collins, D., Conaty, A., Da Silva, A., Gu, W., Joiner, J., Koster, R. D., Lucchesi, R., Molod, A., Owens, T., Pawson, S., Pegion, P., Redder, C. R., Reichle, R., Robertson, F. R., Ruddick, A. G., Sienkiewicz, M. and Woollen, J.: MERRA: NASA's modern-era retrospective analysis for research and applications, J. Clim., 24(14), 3624–3648, doi:10.1175/JCLI-D-11-00015.1, 2011.

Revision 2.9.2019 11:07
Gelöscht: . Discuss.,

Revision 2.9.2019 11:07
Gelöscht: (August), 1–29

Revision 2.9.2019 11:07
Gelöscht: 2018-242, 2018

Rödenbeck, C.: Estimating CO_2 sources and sinks from atmospheric mixing ratio measurements using a global inversion of atmospheric transport. Technical report, Max-Planck-Institute for Biogeochemistry, Jena., 2005.

Rödenbeck, C., Houweling, S., Gloor, M. and Heimann, M.: CO_2 flux history 1982–2001 inferred from atmospheric data using a global inversion of atmospheric transport, Atmos. Chem. Phys., 3, 1919–1964, doi:10.5194/acp-3-1919-2003, 2003.

Rödenbeck, C., Conway, T. J. and Langenfelds, R. L.: The effect of systematic measurement errors on atmospheric CO_2 inversions: a quantitative assessment, Atmos. Chem. Phys., 6(6), 149–161, doi:10.5194/acp-6-149-2006, 2006.

Schuur, E. A. G., Abbott, B. W., Bowden, W. B., Brovkin, V., Camill, P., Canadell, J. G., Chanton, J. P., Chapin, F. S., Christensen, T. R., Ciais, P., Crosby, B. T., Czimczik, C. I., Grosse, G., Harden, J., Hayes, D. J., Hugelius, G., Jastrow, J. D., Jones, J. B., Kleinen, T., Koven, C. D., Krinner, G., Kuhry, P., Lawrence, D. M., McGuire, A. D., Natali, S. M., O'Donnell, J. A., Ping, C. L., Riley, W. J., Rinke, A., Romanovsky, V. E., Sannel, A. B. K., Schädel, C., Schaefer, K., Sky, J., Subin, Z. M., Tarnocai, C., Turetsky, M. R., Waldrop, M. P., Walter Anthony, K. M., Wickland, K. P., Wilson, C. J. and Zimov, S. A.: Expert assessment of vulnerability of permafrost carbon to climate change, Clim. Change, 119(2), 359–374, doi:10.1007/s10584-013-0730-7, 2013.

Schuur, E. A. G., McGuire, A. D., Schädel, C., Grosse, G., Harden, J. W., Hayes, D. J., Hugelius, G., Koven, C. D., Kuhry, P., Lawrence, D. M., Natali, S. M., Olefeldt, D., Romanovsky, V. E., Schaefer, K., Turetsky, M. R., Treat, C. C. and Vonk, J. E.: Climate change and the permafrost carbon feedback, Nature, 520(7546), 171–179, doi:10.1038/nature14338, 2015.

Shakhova, N. E., Semiletov, I. P., Leifer, I., Sergienko, V., Salyuk, A., Kosmach, D., Chernykh, D., Stubbs, C., Nicolsky, D., Tumskoy, V. and Gustafsson, Ö.: Ebullition and storm-induced methane release from the East Siberian Arctic Shelf, Nat. Geosci., 7(1), 64–70, doi:10.1038/ngeo2007, 2014.

Skamarock, W. C., Klemp, J. B., Dudhi, J., Gill, D. O., Barker, D. M., Duda, M. G., Huang, X.-Y., Wang, W. and Powers, J. G.: A Description of the Advanced Research WRF Version 3. NCAR Technical Note NCAR/TN-475+STR., 2008.

Stavert, A. R., O'Doherty, S., Stanley, K., Young, D., Manning, A. J., Lunt, M. F., Rennick, C. and

Arnold, T.: UK greenhouse gas measurements at two new tall towers for aiding emissions verification, Atmos. Meas. Tech., 12(8), 4495–4518, doi:10.5194/amt-12-4495-2019, 2019.

Stull, R. B.: An Introduction to Boundary Layer Meteorology, Springer Netherlands, Dordrecht., 1988.

Sweeney, C., Dlugokencky, E., Miller, C. E., Wofsy, S., Karion, A., Dinardo, S., Chang, R. Y.-W., Miller, J. B., Bruhwiler, L., Crotwell, A. M., Newberger, T., McKain, K., Stone, R. S., Wolter, S. E., Lang, P. E. and Tans, P.: No significant increase in long-term CH_4 emissions on North Slope of Alaska despite significant increase in air temperature, Geophys. Res. Lett., 43(12), 6604–6611, doi:10.1002/2016GL069292, 2016.

Taylor, J. R.: An Introduction to Error Analysis, 2nd Editio., University Science Books, Sausalito, CA., 1997.

Thompson, R. L., Sasakawa, M., Machida, T., Aalto, T., Worthy, D. E. J., Lavric, J. V., Lund Myhre, C. and Stohl, A.: Methane fluxes in the high northern latitudes for 2005–2013 estimated using a Bayesian atmospheric inversion, Atmos. Chem. Phys., 17(5), 3553–3572, doi:10.5194/acp-17-3553-2017, 2017.

Thoning, K. W., Tans, P. P. and Komhyr, W. D.: Atmospheric carbon dioxide at Mauna Loa Observatory: 2. Analysis of the NOAA GMCC data, 1974–1985, J. Geophys. Res., 94(D6), 8549, doi:10.1029/JD094iD06p08549, 1989.

Thornton, B. F., Geibel, M. C., Crill, P. M., Humborg, C. and Mörth, C. M.: Methane fluxes from the sea to the atmosphere across the Siberian shelf seas, Geophys. Res. Lett., 43(11), 5869–5877, doi:10.1002/2016GL068977, 2016.

Vickers, D. and Mahrt, L.: Quality Control and Flux Sampling Problems for Tower and Aircraft Data, J. Atmos. Ocean. Technol., 14(3), 512–526, doi:10.1175/1520-0426(1997)014<0512:QCAFSP>2.0.CO;2, 1997.

Weatherall, P., Marks, K. M., Jakobsson, M., Schmitt, T., Tani, S., Arndt, J. E., Rovere, M., Chayes, D., Ferrini, V. and Wigley, R.: A new digital bathymetric model of the world's oceans, Earth Sp. Sci., 2(8), 331–345, doi:10.1002/2015EA000107, 2015.

WMO: 18th WMO/IAEA Meeting on Carbon Dioxide, Other Greenhouse Gases and Related Tracers Measurement Techniques (GGMT-2015). [online] Available from: https://library.wmo.int/opac/doc_num.php?explnum_id=3074, 2016.

Revision 2.9.2019 11:07
Gelöscht: . J

Revision 2.9.2019 11:07
Gelöscht: . C

Revision 2.9.2019 11:07
Gelöscht: . J

Revision 2.9.2019 11:07
Gelöscht: . P

Revision 2.9.2019 11:07
Gelöscht: CH 4

Revision 2.9.2019 11:07
Gelöscht: 1–8

El Yazidi, A., Ramonet, M., Ciais, P., Broquet, G., Pison, I., Abbaris, A., Brunner, D., Conil, S., Delmotte, M., Gheusi, F., Guerin, F., Hazan, L., Kachroudi, N., Kouvarakis, G., Mihalopoulos, N., Rivier, L. and Serça, D.: Identification of spikes associated with local sources in continuous time series of atmospheric CO, CO_2 and CH_4, Atmos. Meas. Tech., 11(3), 1599–1614, doi:10.5194/amt-11-1599-2018, 2018.

Yver Kwok, C., Laurent, O., Guemri, A., Philippon, C., Wastine, B., Rella, C. W., Vuillemin, C., Truong, F., Delmotte, M., Kazan, V., Darding, M., Lebègue, B., Kaiser, C., Xueref-Remy, I. and Ramonet, M.: Comprehensive laboratory and field testing of cavity ring-down spectroscopy analyzers measuring H_2O, CO_2, CH_4 and CO, Atmos. Meas. Tech., 8(9), 3867–3892, doi:10.5194/amt-8-3867-2015, 2015.

Zona, D., Gioli, B., Commane, R., Lindaas, J., Wofsy, S. C., Miller, C. E., Dinardo, S. J., Dengel, S., Sweeney, C., Karion, A., Chang, R. Y.-W., Henderson, J. M., Murphy, P. C., Goodrich, J. P., Moreaux, V., Liljedahl, A., Watts, J. D., Kimball, J. S., Lipson, D. A. and Oechel, W. C.: Cold season emissions dominate the Arctic tundra methane budget, Proc. Natl. Acad. Sci., 113(1), 40–45, doi:10.1073/pnas.1516017113, 2016.